nature communications

Article

https://doi.org/10.1038/s41467-024-52569-y

SUMOylation of Warts kinase promotes neural stem cell reactivation

Received: 28 November 2023

Accepted: 12 September 2024

Published online: 17 October 2024

Check for updates

Yang Gao[1], Ye Sing Tan[1], Jiaen Lin[1], Liang Yuh Chew[1], Htet Yamin Aung[1], Brinda Palliyana[1], Mahekta R. Gujar[1], Kun-Yang Lin[1], Shu Kondo[2] & Hongyan Wang[1,3,4]

A delicate balance between neural stem cell (NSC) quiescence and proliferation is important for adult neurogenesis and homeostasis. Small ubiquitin-related modifier (SUMO)-dependent post-translational modifications cause rapid and reversible changes in protein functions. However, the role of the SUMO pathway during NSC reactivation and brain development is not established. Here, we show that the key components of the SUMO pathway play an important role in NSC reactivation and brain development in *Drosophila*. Depletion of SUMO/Smt3 or SUMO conjugating enzyme Ubc9 results in notable defects in NSC reactivation and brain development, while their overexpression leads to premature NSC reactivation. Smt3 protein levels increase with NSC reactivation, which is promoted by the Ser/Thr kinase Akt. Warts/Lats, the core protein kinase of the Hippo pathway, can undergo SUMO- and Ubc9-dependent SUMOylation at Lys766. This modification attenuates Wts phosphorylation by Hippo, leading to the inhibition of the Hippo pathway, and consequently, initiation of NSC reactivation. Moreover, inhibiting Hippo pathway effectively restores the NSC reactivation defects induced by SUMO pathway inhibition. Overall, our study uncovered an important role for the SUMO-Hippo pathway during *Drosophila* NSC reactivation and brain development.

Neural stem cells (NSCs) are important for the development and regeneration of the nervous system. While the majority of NSCs in an adult mammalian brain exist in a quiescent state[1,2], extrinsic signals can induce their proliferation, in a process named reactivation. Variants of human orthologs of several genes that regulate NSC reactivation in *Drosophila*, such as IGF1-R, are associated with neurodevelopmental disorders[3–11].

Drosophila NSCs, also known as neuroblasts, have emerged as a powerful model system to study the mechanisms underlying NSC reactivation in vivo[12,13]. *Drosophila* NSCs in the central brain (CB) and thoracic ventral nerve cord (VNC) enter into quiescence at the end of embryogenesis, and subsequently exit quiescence (reactivate) in response to dietary amino acids, typically within 24 h after larval hatching (h ALH) (Fig. 1a)[14–16]. The nutritional signals originate from the *Drosophila* fat body—functional equivalent of mammalian liver and adipose tissue[17]—and lead to activation of the insulin/insulin-like growth factor (IGF) signaling pathway[18,19] and inactivation of the Hippo signaling pathway in NSCs for their reactivation[18–21].

The evolutionarily-conserved Hippo pathway maintains NSC quiescence in *Drosophila* larval brains[20,22]. The core Hippo pathway consists of a kinase cascade, in which Hippo (Hpo)/Mst1/2 phosphorylates Warts (Wts)/Lats1/2. When activated, Wts/Lats1/2

[1]Neuroscience and Behavioral Disorders Programme, Duke-NUS Medical School, Singapore, Singapore. [2]Department of Biological Science and Technology, Faculty of Advanced Engineering, Tokyo University of Science, Niijuku, Katsushika-ku, Tokyo, Japan. [3]Department of Physiology, Yong Loo Lin School of Medicine, National University of Singapore, Singapore, Singapore. [4]NUS Graduate School - Integrative Sciences and Engineering Programme (ISEP), National University of Singapore, Singapore, Singapore. e-mail: hongyan.wang@duke-nus.edu.sg

https://doi.org/10.1038/s41467-024-52569-y

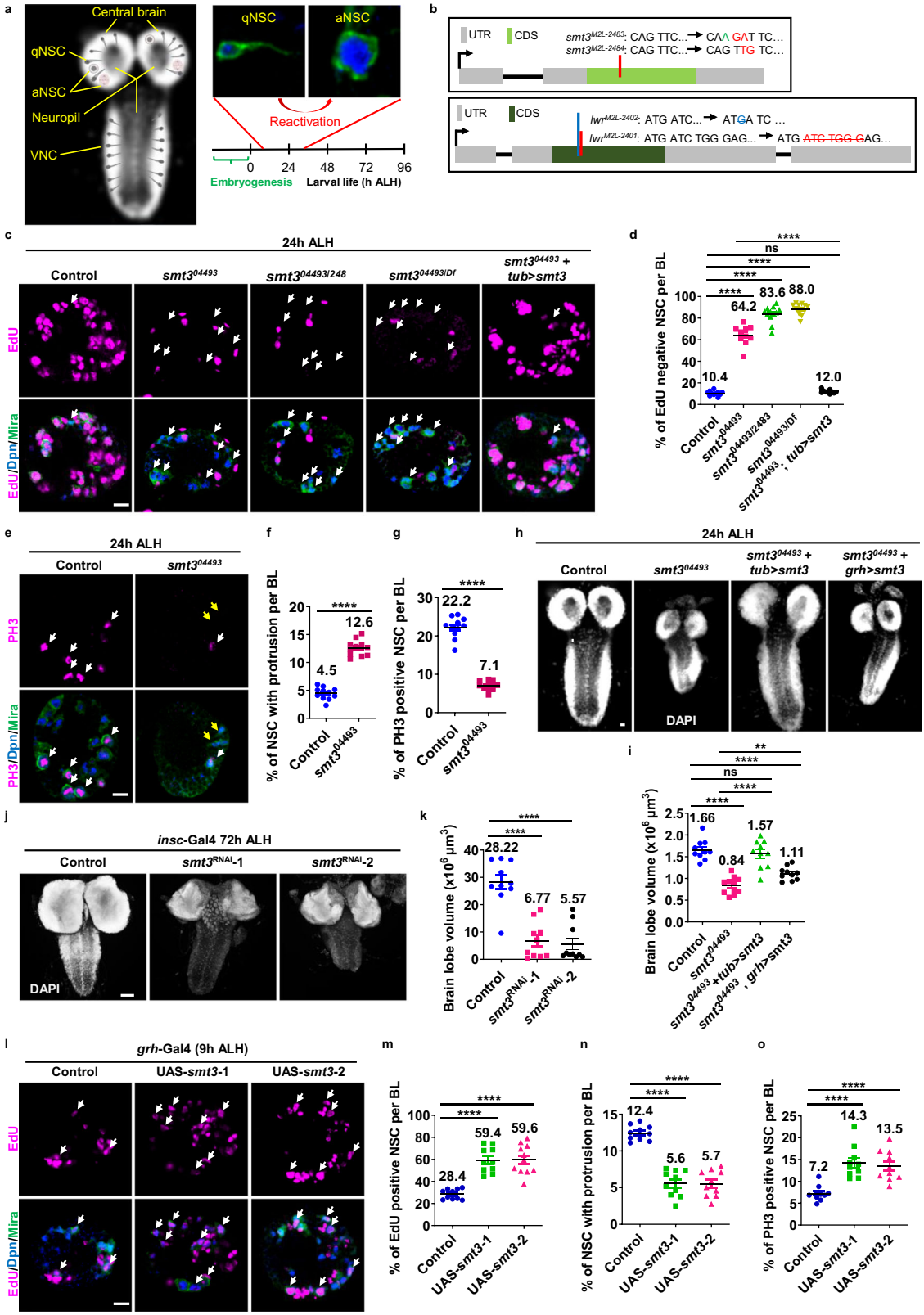

phosphorylates the oncogenic transcriptional coactivator Yorkie (Yki)/YAP, resulting in its cytoplasmic retention[23]. When the Hippo pathway is inactive, Yki enters the nucleus to enhance the expression of target genes[23–25]. A CRL4 E3 ubiquitin ligase promotes Wts kinase ubiquitination and degradation, thus promoting NSC reactivation[26]. The intricate interplay between the InR/PI3K/Akt and Hippo pathways during NSC reactivation is coordinated by components of the Striatin-interacting phosphatase and kinase (STRIPAK) complexes[27]. Moreover, various intrinsic molecules are required for NSC reactivation[28–33].

SUMOylation is a type of post-translational modification in which the small ubiquitin-related modifier (SUMO) peptide is conjugated to a substrate protein for swift and reversible alteration of protein function, including its activity, stability, or subcellular localization[34,35]. In

Fig. 1 | Smt3, the single SUMO protein in *Drosophila*, is required for NSC reactivation and brain development. a Diagrammatic representation of *Drosophila* brain and quiescent NSC reactivation time line. aNSC: active NSC, qNSC: quiescent NSC. **b** Diagram of CRISPR-Cas9 mediated gene deletion mutants on *smt3* and *lwr*. **c** Larval brain lobes from control (*yw*), $smt3^{04493}$, $smt3^{04493}/smt3^{M2L\text{-}2483}$, $smt3^{04493}/smt3^{Df24652}$ and $smt3^{04493}$+*tub*>*smt3* were analyzed for EdU incorporation. NSCs were marked by Dpn and Mira. White arrows point to EdU- qNSCs. **d** Quantification of EdU- NSCs per brain lobe (BL) for (**c**). Control, 10.4 ± 2.2, n = 11; $smt3^{04493}$, 64.2 ± 8.9, P = 5.6E-14, n = 10; $smt3^{04493}/smt3^{M2L\text{-}2483}$, 83.6 ± 7.7, P = 8.9E-09, n = 12; $smt3^{04493}/smt3^{Df24652}$, 88 ± 5.2, P = 2.6E-10, *n* = 12; $smt3^{04493}$ + *tub*>*smt3*, 12 ± 1.6, *p* = 0.07, P = 5.0E-13, n = 10. **e** Larval brain lobes from control (*yw*) and $smt3^{04493}$ were labeled with Dpn, PH3 and Mira. White arrows point to PH3+ NSCs, yellow arrows point to qNSCs with protrusion. **f** Quantification of NSCs retaining cellular protrusion per BL for (**e**). Control, 4.5 ± 1.1, n = 11; $smt3^{04493}$, 12.6 ± 1.4, P = 8.5E-14, n = 11. **g** Quantification of PH3+ NSCs per BL for (**e**). Control, 22.2 ± 2.7, P = 3.5E-13, n = 11; $smt3^{04493}$, 7.1 ± 1.2, n = 11. **h** Maximum intensity z-projection of larval brains from control (*yw*), $smt3^{04493}$, $smt3^{04493}$+*tub*>*smt3*, and $smt3^{04493}$+*grh*>*smt3* were stained with DAPI. **i** Quantification of brain volume in (**h**). Control, 1.66 ± 0.23, n = 10; $smt3^{04493}$, 0.84 ± 0.19, P = 4.4E-08, n = 11; $smt3^{04493}$+*tub*>*smt3*, 1.57 ± 0.32, P = 0.48, n = 10; $smt3^{04493}$+*grh*>*smt3*, 1.11 ± 0.15, P = 8.3E-06, n = 10. **j** Larval brain lobes in control (β-gal^{RNAi}) and $smt3^{RNAi}$ lines driven by *insc*-Gal4 were stained with DAPI. **k** Quantification of brain volume in (**j**). Control, 28.22 ± 8.2, n = 10; $smt3^{RNAi}$-1, 6.77 ± 6.6, P = 2.5E-06, n = 10; $smt3^{RNAi}$-2, 5.57 ± 6.7, P = 4.6E-06, n = 11. **l** Larval brain lobes in control (β-gal^{RNAi}) and two UAS-venus-*smt3* lines driven by *grh*-Gal4 were analyzed for EdU incorporation. White arrows point to EdU+ NSCs. **m** Quantification of EdU+ NSCs per BL in (**j**). Control, 28.4 ± 4.6, n = 10; UAS-venus-*smt3*-1, 59.4 ± 11.3, P = 2.3E-07, n = 10; venus-*smt3*-2, 59.6 ± 13.3, P = 1.0E-06, n = 11. **n** Quantification of NSCs retaining cellular protrusion per BL in (**j**). Control, 12.4 ± 1, n = 10; UAS-venus-*smt3*-1, 5.6 ± 1.8, P = 4.0E-09, n = 10; venus-*smt3*-2, 5.7 ± 2, P = 2.3E-08, n = 10. **o** Quantification of PH3+ NSCs per BL in (**j**). Control, 7.2 ± 1.7, n = 10; UAS-venus-*smt3*-1, 14.3 ± 3.6, P = 2.9E-05n = 10; venus-*smt3*-2, 13.5 ± 3.5, P = 7.0E-05, n = 10. Data are presented as mean ± SD. **** for P ≤ 0.0001, ns for P > 0.05. Scale bars are 10 μm except in (**j**), which is 50 μm.

Drosophila, there exists a single *SUMO* gene known as *smt3*. SUMO maturation involves removal of the C-terminal extension by Ubiquitin-Like Protease 1 (Ulp1) that exposes its diglycine motif[36,37]. After maturation, SUMO is activated by the heterodimeric SUMO-activating enzyme (SUMO E1) Aos1/Uba2, through the formation of a thioester bond[38,39]. Subsequently, this thioester linkage is transferred to a cysteine in the sole E2-conjugating enzyme ubiquitin-conjugating 9 (Ubc9, encoded by the *lesswright* (*lwr*) gene)[39–42]. Ultimately, Ubc9 transfers SUMO to the substrate protein, through an isopeptide bond between the lysine residue of the substrate and the C-terminal glycine in SUMO[40–42]. SUMO E3 ligases, which bind both Ubc9 and the substrate protein, facilitate the formation of isopeptide bonds[34,43–45]. The SUMO pathway plays a pivotal role in developmental processes[34,46,47], and its dysregulation is implicated in a variety of human diseases, including cancers and neurodegenerative diseases[47–52]. However, the role of the SUMO pathway during NSC reactivation and brain development remains to be established.

In this study, we demonstrated an important, indispensable role for the SUMO pathway in NSC reactivation and brain development.

Results

Smt3, the single SUMO protein in *Drosophila*, is required for NSC reactivation and brain development

To identify regulators of NSC lineage development, we carried out a genetic screen using a collection of 504 CRISPR-Cas9-mediated gene deletion mutants on chromosome 2L[53]. From this screen, we isolated four mutants, M2L-2483, M2L-2484, M2L-2401 and M2L-2402, that displayed defects in NSC reactivation (Supplementary Fig 1a, b). At 24 h ALH, the majority of NSCs in control larval brain were reactivated and incorporated with 5-ethynyl-2'-deoxyuridine (EdU), with only 9.6% of NSCs remaining quiescent and negative for EdU (Supplementary Fig 1a, b). In contrast, the percentage of quiescent NSCs that were EdU-negative was significantly higher at 28.0% and 28.8% in M2L-2483 and M2L-2484 heterozygous mutants, respectively, and at 47.8% and 42.6% in M2L-2401 and M2L-2402 homozygous mutants, respectively (Supplementary Fig 1a, b). The M2L-2483 and M2L-2484 mutants contained mutations in *smt3*/*SUMO*, which encodes the solo SUMO protein in *Drosophila*, whereas the M2L-2401 and M2L-2402 mutants contained mutations in *lwr*/*Ubc9*, which encodes the SUMO E2 conjugating enzyme Ubc9 in *Drosophila*. M2L-2483, M2L-2484, M2L-2401 and M2L-2402 are hereinafter termed $smt3^{M2L\text{-}2483}$, $smt3^{M2L\text{-}2484}$, $lwr^{M2L\text{-}2401}$ and $lwr^{M2L\text{-}2402}$, respectively. The mutation in $smt3^{M2L\text{-}2483}$ is a result of a silent mutation on Q26 and the addition of 2 extra base pairs (bps), which results in a missense mutation from the 27th amino acid onwards (Fig. 1b, Supplementary Table 1a). The mutation in $smt3^{M2L\text{-}2484}$ is a result of the addition of two extra nucleotide bases, leading to a missense mutation from 27th amino acid and early termination of translation at 34th amino acid (Fig. 1b, Supplementary Table 1a). Furthermore, mutations in $lwr^{M2L\text{-}2401}$ and $lwr^{M2L\text{-}2402}$ are caused by a 7- and 1-bp deletions, resulting in missense mutations from the 40th or 39th amino acids, respectively, and early termination of translation at 59th and 61th amino acids, respectively (Fig. 1b, Supplementary Table 1b).

Since $smt3^{M2L\text{-}2483}$ and $smt3^{M2L\text{-}2484}$ mutants were homozygous lethal at 24 h ALH, we examined a known *smt3* loss-of-function allele, $smt3^{04493}$, which was generated by a P-element insertion at 20 bp upstream of the transcription start site and survived to early second instar stage[54]. At 24 h ALH, 64.2% of NSCs in $smt3^{04493}$ homozygous mutants failed to incorporate EdU as compared to 10.4% in control larval brains (Fig. 1c, d). Furthermore, the percentage of EdU-negative, quiescent NSCs in a trans-heterozygous mutant between $smt3^{04493}$ and $smt3^{M2L\text{-}2483}$ and a hemizygous mutant between $smt3^{04493}$ and a *smt3*-deficient line ($smt3^{Df24652}$) dramatically increased to 83.6% and 88%, respectively (Fig. 1c, d). We further quantified the percentage of quiescent NSCs with primary cellular protrusions, the hallmark of quiescent NSCs[21,55]. Using Miranda (Mira) as a marker for the cellular extensions, we found that there was a significant percentage of Mira-positive NSCs that still extended their cellular protrusions in $smt3^{04493}$ mutant brains (12.6%) as compared to 4.5% in control larval brains (Fig. 1e, f). Moreover, the number of mitotic NSCs that are positive for phospho-Histone H3 (PH3) was significantly reduced from 22.2% in control larval brains to 7.1% in $smt3^{04493}$ mutant brains (Fig. 1e, g). Smt3 fluorescence intensity was significantly reduced to 0.52-fold in $smt3^{04493}$ mutant NSCs as compared to control NSCs (Supplementary Fig 1c, d), which validated $smt3^{04493}$ as a loss-of-function allele. Additionally, at 24 h ALH, knockdown of *smt3* in NSCs by two independent RNAi lines resulted in prominent reactivation defects in NSCs: the percentage of EdU-negative quiescent NSCs significantly increased from 8.8% in control larval brains to 53.2% and 58.5% in $smt3^{RNAi}$ lines respectively (Supplementary Fig 1e, f). Both $smt3^{RNAi}$ lines still displayed strong NSC reactivation defects at 48 h and 72 h ALH at 29 °C (Supplementary Fig 3a, b), suggesting a block in NSC reactivation. Upon *smt3* knockdown in NSCs, only 34.7% and 17.9% of the NSCs were Smt3/SUMO-positive in these two RNAi stocks, compared with 100% in control NSCs, confirming the efficiency of *smt3* knockdown (Supplementary Fig 1g, h). While $smt3^{04493}$ mutant had a decrease in the total NSC number (68 NSCs/brain lobe vs 87.1 in control), the total number of NSCs in both $smt3^{RNAi}$ lines appears to be normal (82.3 and 79.3 vs 83.3 in control; Supplementary Table 2).

Remarkably, the volume of $smt3^{04493}$ mutant brain lobes was dramatically reduced to $0.84 \times 10^6\ \mu m^3$, compared to control larval brain volume of $1.66 \times 10^6\ \mu m^3$ (Fig. 1h, i), mimicking microcephaly phenotypes. There was a significant decrease in the number of Dpn-positive neuroblasts at 4 h after egg laying in $smt3^{04493}$ homozygous embryos (Supplementary Fig 1i, j), suggesting that this embryonic phenotype

may also contribute to the reduction of brain lobe size in *smt3* mutants. These data indicate that Smt3/SUMO is required for NSC reactivation and brain development.

Overexpression of *smt3/SUMO* leads to premature NSC reactivation

We generated Venus-tagged *smt3* transgenic flies and verified them with anti-SUMO and anti-Venus antibodies (Supplementary Fig 1l, m). At 9 h ALH, most of the wild-type NSCs were still in a quiescent state, with only about 28.4% of NSCs incorporating EdU (Fig. 1l, m). Remarkably, overexpression of Venus-tagged *smt3* by NSC-specific driver *grainy head*-Gal4 (*grh*-Gal4) significantly increased the percentage of proliferative NSCs marked by EdU incorporation: from 28.4% in control to 59.4% and 59.6% in two independent *smt3* overexpression strains (Fig. 1l, m). Moreover, the percentage of quiescent NSCs with primary cellular protrusions significantly decreased from 12.4% in control to 5.6% and 5.7% in *smt3* overexpression strains (Fig. 1n). In addition, the percentage of PH3-positive mitotic NSCs significantly increased from 7.2% in control to 14.3% and 13.5% in *smt3* overexpression strains (Fig. 1o), suggesting that *smt3/SUMO* overexpression triggers premature NSC reactivation. Furthermore, overexpression of Venus-tagged *smt3* driven by *tubulin*-Gal4 (*tub*-Gal4) fully rescued NSC reactivation defects (Fig. 1c, d), microcephaly-like phenotypes (Fig. 1h, i) and Smt3/SUMO intensity (Supplementary Fig 1n, o) in $smt3^{04493}$ allele, suggesting that Venus-tagged Smt3 is functional. Overexpression of *smt3* driven by *grh*-Gal4 partially rescued the microcephaly-like phenotypes (Fig. 1h, i) in $smt3^{04493}$ allele, suggesting that NSC reactivation phenotype contributes to the microcephaly phenotype in *smt3* mutant. *grh*-Gal4 drives the expression of UAS transgenes in only a subset but not all NSCs in both embryonic ventral nerve cord (Supplementary Fig 1k) and larval brains[18], which likely accounts for the incomplete rescue of the microcephaly-like phenotypes using this driver. Indeed, knocking down of *smt3* using another NSC-specific driver *insc*-Gal4, which is known to drive expression in all NSCs, but not *grh*-Gal4, dramatically decreased the brain size at 72 h ALH, causing microcephaly-like phenotype (Fig. 1j, k), consistent with *smt3* mutant phenotype. Upon overexpression of *smt3* or *lwr* at 9 h ALH, there was a slight increase in NSC number, compared with the UAS control line (Supplementary Table 2). Taken together, our results indicate that Smt3/SUMO is both necessary and sufficient for promoting NSC reactivation and indispensable for brain development.

SUMO conjugating enzyme Lwr/Ubc9 promotes NSC reactivation

To further understand the role of the SUMO conjugating enzyme Ubc9/Lwr in *Drosophila*, we analyzed two other *lwr* loss of function alleles, lwr^{05486} and lwr^{13}, both of which were generated from the imprecise excision of a P-element inserted in the regulatory zone[56,57]. Interestingly, at 24 h ALH, 60.5% of NSCs in lwr^{05486} and 55.2% of NSCs in lwr^{13} mutants failed to incorporate EdU as compared to 9% in control (Fig. 2a, b), suggesting severe NSC reactivation defects in these mutants. In addition, the percentage of quiescent NSCs retaining the primary cellular protrusion increased significantly from 4.5% in control to 12.9% and 12.1% in lwr^{05486} and lwr^{13} mutant brains, respectively (Fig. 2c). Moreover, the number of PH3-positive mitotic NSCs was greatly reduced from 23.4% in control to 15% in lwr^{05486} and 15.3% in lwr^{13} mutant brains (Fig. 2d). lwr^{13} mutant brains showed a mild decrease in NSC number (79.2 vs 87.1 in control; Supplementary Table 2). Additionally, knockdown of *lwr* in NSCs by two independent RNAi lines also resulted in NSC reactivation defects at 24 h ALH, wherein, the percentage of EdU-negative NSCs significantly increased from 4.9% in control to 36.8% and 30.8% in the two lwr^{RNAi} lines (Supplementary Fig 2a, b). lwr^{13} still exhibited NSC reactivation defects at 48 h, 72 h and 96 h ALH at 25 °C (Supplementary Fig 3c, d), suggesting a failure of NSC reactivation.

Consistent with NSC reactivation defects in *lwr* mutants, the volume of the brain lobes significantly reduced from $1.66 \times 10^6\ \mu m^3$ in control to $1.06 \times 10^6\ \mu m^3$ in lwr^{13} mutant at 24 h ALH (Fig. 2e, f). The microcephaly-like phenotype of lwr^{13} mutants was more severe at 96 h ALH ($34.98 \times 10^7\ \mu m^3$ vs $3.88 \times 10^7\ \mu m^3$ in control, Supplementary Fig 3e, f). These data suggest that *lwr* is important for the reactivation of quiescent NSCs and brain development.

Overexpression of SUMO E2 Lwr/Ubc9 drives premature exit of NSC quiescence

Overexpression of *lwr* in NSCs at 9 h ALH resulted in premature reactivation of NSCs, evident by a significant increase in the percentage of EdU-positive NSCs from 30.3% in control to 49.2% in *lwr* overexpression strain at 9 h ALH (Fig. 2g, h). Moreover, the percentage of NSCs with primary cellular protrusion dramatically decreased from 12.4% in control brains to 6.3% in *lwr* overexpression brains (Fig. 2i). In addition, the percentage of PH3-positive mitotic NSCs significantly increased from 7.2% in control brains to 12.1% in *lwr* overexpression brains (Fig. 2j). Interestingly, overexpression of a dominant-negative *lwr* (lwr^{DN}) stain[58,59] at 24 h ALH resulted in reactivation defects with increased number of EdU-negative quiescent NSCs (Supplementary Fig 2c, d). Furthermore, the overexpression of wild-type *lwr* driven by *grh*-Gal4 or *tub*-Gal4 in lwr^{13} homozygous mutant at 24 h ALH significantly rescued NSC reactivation defects (Supplementary Fig 2e, f), while overexpression of lwr^{DN} led to more severe NSC reactivation defects (Supplementary Fig 2e, f). Besides, overexpression of *lwr* driven by *tub*-Gal4 and *grh*-Gal4 significantly rescued the microcephaly-like phenotype caused by lwr^{13} mutant (Fig. 2e, f). However, overexpression of *smt3* or *lwr* failed to promote NSC reactivation in sucrose-only food (Supplementary Fig 2g, h), suggesting that Smt3 and Ubc9 promote NSC cell cycle reentry relying on the presence of nutrition. There was no significant difference between control and *smt3* or *lwr* overexpression at 24 h ALH (Supplementary Fig 3g, h), suggesting their overexpression effect was not sustained at a later stage. Taken together, we propose that the SUMO conjugating enzyme Ubc9/Lwr, like the SUMO protein, is a key regulator of NSC reactivation and brain development.

The heterodimeric SUMO activating enzyme Aos1/Uba2 is required for NSC reactivation

Next, we analyzed the functions of the heterodimeric SUMO activating enzyme Aos1/Uba2 during NSC reactivation. A known *aos1* loss of function allele, $aos1^{c06048}$, which was generated by a PiggyBac transposon insertion[60] in the 5′ UTR of the *aos1* gene, 41 bp upstream from the ATG[61], showed obvious NSC reactivation defects (Fig. 2k–n). At 24 h ALH, the percentage of EdU-negative quiescent NSCs significantly increased from 9.4% in control brains to 32.8% in $aos1^{c06048}$ mutant brains (Fig. 2k, l). Furthermore, the percentage of quiescent NSCs retaining primary cellular protrusions increased from 4.4% in control brains to 11.1% in $aos1^{c06048}$ mutant brains (Fig. 2m), and the percentage of PH3-positive mitotic NSCs reduced from 20.8% in control brains to 14.4% in $aos1^{c06048}$ mutant brains (Fig. 2n). Consistently, knockdown of *aos1* by RNAi at 24 h ALH resulted in a significant increase in the number of quiescent NSCs lacking EdU incorporation (Supplementary Fig 2i, j). $aos1^{c06048}$ mutant brains showed a mild decrease in NSC number (80.2 vs 87.1 in control; Supplementary Table 2).

Uba2, the other component of the SUMO E1 heterodimeric enzyme alongside Aos1, is also required for NSC reactivation. Knockdown of *uba2* in NSCs by two independent RNAi lines at 24 h ALH led to a notable increase in the percentage of EdU-negative quiescent NSCs: 6.1% in control to 32.5% and 29.7% in the two knockdown strains (Fig. 2o, p). In addition, the percentage of quiescent NSCs with primary

https://doi.org/10.1038/s41467-024-52569-y

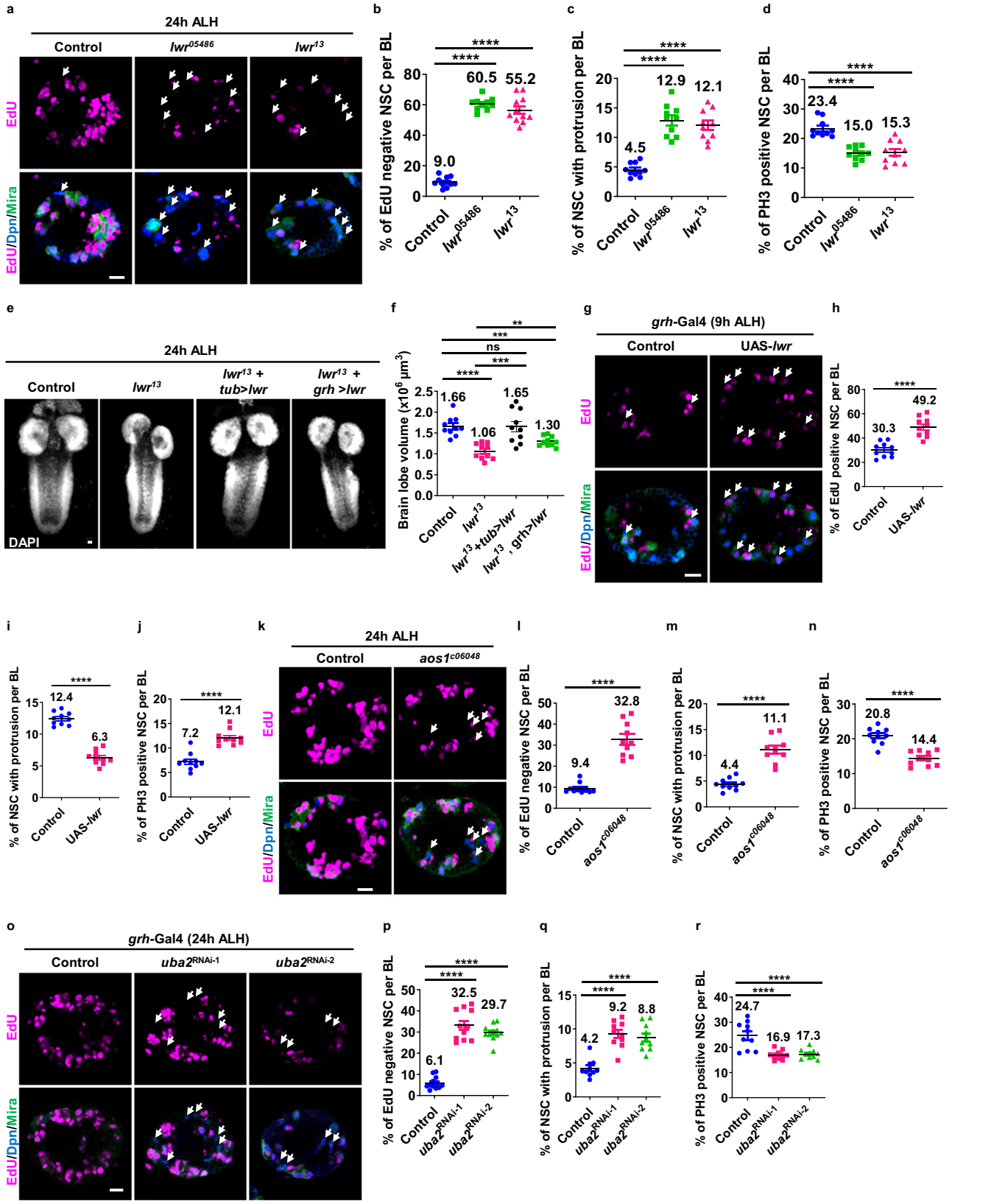

cellular protrusions increased significantly from 4.2% in control to 9.2% and 8.8% in the two *uba2*^{RNAi} lines (Fig. 2q). Alternately, the number of PH3-positive mitotic NSCs reduced from 24.7% in control to 16.9% and 17.3% in *uba2*^{RNAi} lines (Fig. 2r). These findings point to an essential role for the heterodimeric SUMO activating enzyme Aos1/Uba2 in NSC reactivation.

Smt3/SUMO levels increase with NSC reactivation

To assess the expression pattern of *smt3* in larval brains, we analyzed a published dataset of single cell RNA-sequencing obtained from late first instar larvae at 16 h ALH[62]. *smt3* expression level was low in quiescent NSCs, but increased notably in active NSCs (Fig. 3a). Dpn, an NSC marker that has a higher expression level in active than quiescent

Fig. 2 | SUMO E2 and E1 are required for NSC reactivation. a, **k**, **o** At 24 h ALH, larval brain lobes from various genotypes were analyzed for EdU incorporation. NSCs were marked by Dpn and Mira. White arrows point to EdU- qNSCs. **b** Quantification of EdU- NSCs per BL for (**a**). Control (*yw*), 9 ± 3.3, n = 11; lwr^{05486}, 60.5 ± 4.2, P = 8.1E-18, n = 10; lwr^{13}, 55.2 ± 8.5, P = 1.9E-13, n = 11. **c** Quantification for percentage of NSCs retaining cellular protrusion per BL for (**a**). Control, 4.5 ± 1.1, n = 10; lwr^{05486}, 12.9 ± 2.7, P = 4.2E-08, n = 10; lwr^{13}, 12.1 ± 1.6, P = 9.6E-08, n = 10. **d** Quantification of PH3+ NSCs per BL for (**a**). Control, 23.4 ± 3, n = 10; lwr^{05486}, 15 ± 2.2, P = 1.1E-06, n = 10; lwr^{13}, 15.3 ± 3.8, P = 5.1E-05, n = 10. **e** Maximum intensity z-projection of larval brains from control (*yw*), lwr^{13}, lwr^{13}+*tub>lwr* and lwr^{13}+*grh>lwr* were stained with DAPI. **f** Quantification of brain volume for (**e**). Control, 1.66 ± 0.23, n = 10; lwr^{13}, 1.06 ± 0.19, P = 6.9E-06, n = 10; lwr^{13}+*tub>lwr*, 1.65 ± 0.4, P = 0.98, P = 0.0005, n = 10 BL; lwr^{13}+*grh>lwr*, 1.3 ± 0.12, P = 0.0004, P = 0.0038, n = 10. **g** At 9 h ALH, larval brain lobes in control (β-gal^{RNAi}) and UAS-*lwr* line driven by *grh*-Gal4 were analyzed for EdU incorporation. White arrows point to EdU+ NSCs. **h** Quantification of EdU+ NSCs per BL for (**g**). Control, 30.3 ± 6, n = 10; UAS-*lwr*, 49.2 ± 8, P = 2.6E-05, n = 10. **i** Quantification of NSCs retaining cellular protrusion per BL for (**g**). Control, 12.4 ± 1, n = 10; UAS-*lwr*, 6.3 ± 1.1, P = 1.4E-10, n = 10. (**j** Quantification of PH3+ NSCs per BL for (**g**). Control, 7.2 ± 1.7, n = 10; UAS-*lwr*, 12.1 ± 1.5, P = 2.9E-06, n = 10. **l** Quantification of EdU- NSCs per BL for (**k**). Control (*yw*), 9.4 ± 2.5, n = 10 BL; $aos1^{c06048}$, 32.8 ± 8, P = 6.2E-08, n = 10. **m** Quantification of NSCs retaining cellular protrusion per BL for (**k**). Control, 4.4 ± 1.1, n = 10; $aos1^{c06048}$, 11.1 ± 2.4, P = 2.7E-07, n = 10. **n** Quantification of PH3+ NSCs per BL for (**k**). Control, 20.8 ± 2.3, n = 10; $aos1^{c06048}$, 14.4 ± 2, P = 3.5E-06, n = 10. **p** Quantification of EdU- NSCs per BL for (**o**). Control (β-gal^{RNAi}), 6.1 ± 3, n = 11; $uba2^{RNAi}$-1, 32.5 ± 7.1, P = 2.1E-10, n = 11; $uba2^{RNAi}$-2, 29.7 ± 3.8, P = 5.7E-13, n = 11. **q** Quantification of NSCs retaining cellular protrusion per BL for (**o**). Control, 4.2 ± 1.3, n = 10; $uba2^{RNAi}$-1, 9.2 ± 1.9, P = 2.1E-06, n = 10; $uba2^{RNAi}$-2, 8.8 ± 2, P = 8.4E-06, n = 10. **r** Quantification of PH3+ NSCs per BL for (**o**). Control, 24.7 ± 5.4, n = 10; $uba2^{RNAi}$-1, 16.9 ± 1.8, P = 0.0004, n = 10; $uba2^{RNAi}$-2, 17.3 ± 1.9, P = 0.0007, n = 10. Data are presented as mean ± SD. **** for P ≤ 0.0001, *** for P ≤ 0.001, ns indicates p > 0.05. Scale bars: 10 μm.

NSCs[27], was included as a positive control, while *Rpl32*, a housekeeping gene that has similar expression levels in these two cell populations (Fig. 3a). Consistent with changes in mRNA levels, at 6 h ALH, the relative SUMO intensity increased from 1.25 in quiescent NSCs (qNSCs) to 2.57 in active NSCs (aNSCs) (Fig. 3b, c). While at 12 h ALH, the relative SUMO intensity in quiescent NSCs significantly increased to 1.46 (compared with 1.25 at 6 h ALH), the relative SUMO intensity in active NSCs remained relatively constant at 2.45 (Fig. 3b, c). These results suggest that the Smt3/SUMO mRNA and protein levels in quiescent NSCs are increased when quiescent NSCs re-enter the cell cycle but remain constant following the reactivation.

Akt promotes the increase of Smt3/SUMO protein during NSC reactivation

To test whether InR/PI3K/Akt pathway regulates SUMO protein during NSC reactivation, we examined the SUMO protein levels in akt^3 mutant[63] larva brains. SUMO protein level at 24 h ALH significantly decreased to 0.65-fold in akt^3 mutant compare to control (Fig. 3d, e). Consistent with this observation, the SUMO fluorescence intensity in both quiescent NSCs and active NSCs in akt^3 is significantly lower than that in control (0.82-fold vs 1-fold in quiescent NSCs, 1.49-fold vs 1.96-fold in active NSCs, Fig. 3f, g). Quantitative real-time PCR revealed no significant change in *smt3* mRNA levels in akt^3 mutant larval brains compared to control at 24 h ALH (Fig. 3h), suggesting that Akt promotes Smt3 protein levels, but not transcript levels. On the contrary, overexpression of an active form of *akt* (Myr-*Akt*) in NSCs led to significant increase of SUMO intensity in both quiescent NSCs and active NSCs compared to control (Fig. 3i, j; 1.32-fold vs 1-fold in quiescent NSCs and 2.39-fold vs 1.59-fold in active NSCs). Moreover, overexpression of an active form of *InR* (InR^{AD}), the Akt upstream activator driven by *grh*-Gal4 led to significant increase of SUMO intensity in both quiescent NSCs and active NSCs compared to control (1.14-fold vs 1-fold in quiescent NSCs and 2.05-fold vs 1.59-fold in active NSCs, Fig. 3i, j). Besides, the percentage of NSCs with higher SUMO intensity per brain lobe in these brains are significantly higher (Fig. 3i, k). While *Arf1* overexpression promotes NSC reactivation via the regulation of microtubule growth[32], it did not affect SUMO intensity (Supplementary Fig. 4a, b). These results suggest that InR/Akt specifically promotes the increase of SUMO protein during NSC reactivation to promote quiescent NSCs reentering cell cycle.

SUMO pathway promotes Wts SUMOylation at Lys766

Utilizing the Joined Advanced SUMOylation Site and Sim Analyser (JASSA)[64], Wts-Lys766 (Wts-K766) and Wts-Lys561 (Wts-K561) were predicted to be SUMOylated with a high probability. Wts-K766 resides in the kinase domain (Supplementary Table 3a; Fig. 4a) within the consensus sequence [Ψ]-[K]-[x]-[E/D]-[x]-[E/D]$_6$ (ψ stands for a hydrophobic amino acid, Supplementary Table 3b), which belongs to NDSM (negatively charged amino acid-dependent SUMOylation site)[65]. Wts-K561 is within the consensus sequence [E/D]-[x]-[K]-[Ψ] (Supplementary Table 3b), an inverted SUMOylation motif[66]. Since Wts-K766, but not Wts-K561, is conserved in human LATS1 and LATS2 (Supplementary Table 3c), we focused on Wts-K766 in our subsequent study. To investigate whether Wts can be SUMOylated, we conducted SUMOylation assays in S2 cells. Cells were transiently transfected with Flag-Wts (~150 kD), either alone or in combination with Myc-tagged wild-type (WT) Smt3. Following precipitation with a Flag antibody, the resulting protein complexes exhibited an anticipated >150 kD bands corresponding to SUMOylated Flag-Wts (Fig. 4b). Notably, *smt3* overexpression resulted in a remarkable 2.59-fold increase in SUMOylated Flag-Wts levels (Fig. 4b, c), suggesting that Smt3 promotes Wts SUMOylation. It is noteworthy that the conjugation of Smt3 with target proteins relies on its two carboxy-terminal glycine residues, G87 and G88 (Supplementary Table 1a in yellow color). Substituting these two amino acids with alanine (G87A, G88A) is sufficient to disrupt this conjugation[67,68]. Consistently, when Flag-Wts and Myc-$Smt3^{G87A,\ G88A}$ (denoted as Myc-$Smt3^{AA}$) were co-expressed in S2 cells, we observed a significantly reduced enhancement of Flag-Wts SUMOylation from 2.59-fold to 1.28-fold (Fig. 4b, c). These results highlight the specificity of Wts SUMOylation by Smt3.

Overexpression of *wts* in NSCs resulted in obvious increase of Wts intensity in NSCs (1.7-fold compared to 1-fold in control, Supplementary Fig 5a, b), while Wts intensity decreased dramatically to 0.69-fold of control in $wts^{e26\text{-}1}$ mutant NSCs (Supplementary Fig 5c, d). In addition, in S2 cells upon *wts* knockdown, Wts protein level decreased to 0.36-fold in Western blot (Supplementary Fig 5e, f) and 0.25-fold in immunostaining (Supplementary Fig 5g, h), compared with control groups, respectively, further validating the specificity of anti-Wts antibodies. Moreover, clonal experiments that allowed us to directly compare endogenous Wts signal intensity in wild-type cells with that of neighboring *wts*-depleted or *wts*-overexpressing cells all strongly supported the specificity of anti-Wts antibodies in larval brains (Supplementary Fig 5i–n).

Subsequently, we examined the SUMOylation of endogenous Wts in S2 cells following the depletion of *SUMO*/*smt3* or SUMO E2 *lwr* with double-stranded RNA (dsRNA) treatment. In input, there was a significant reduction in overall SUMOylation in *smt3*- or *lwr*-knockdown groups compared to the control (gfp^{RNAi}) (Fig. 4d). Within the IP samples, the SUMOylation of endogenous Wts decreased significantly from 1-fold in control to 0.64-fold and 0.68-fold, in the *smt3*- and *lwr*- knockdown groups respectively (Fig. 4d, e), indicating that both SUMO and SUMO E2 are essential for Wts SUMOylation. The high efficiency of *smt3* and *lwr* knockdown was confirmed by anti-SUMO blotting of the input samples (Fig. 4d) and anti-HA (Ubc9 tagged with HA) immunostaining (Supplementary Fig 6a), respectively.

https://doi.org/10.1038/s41467-024-52569-y

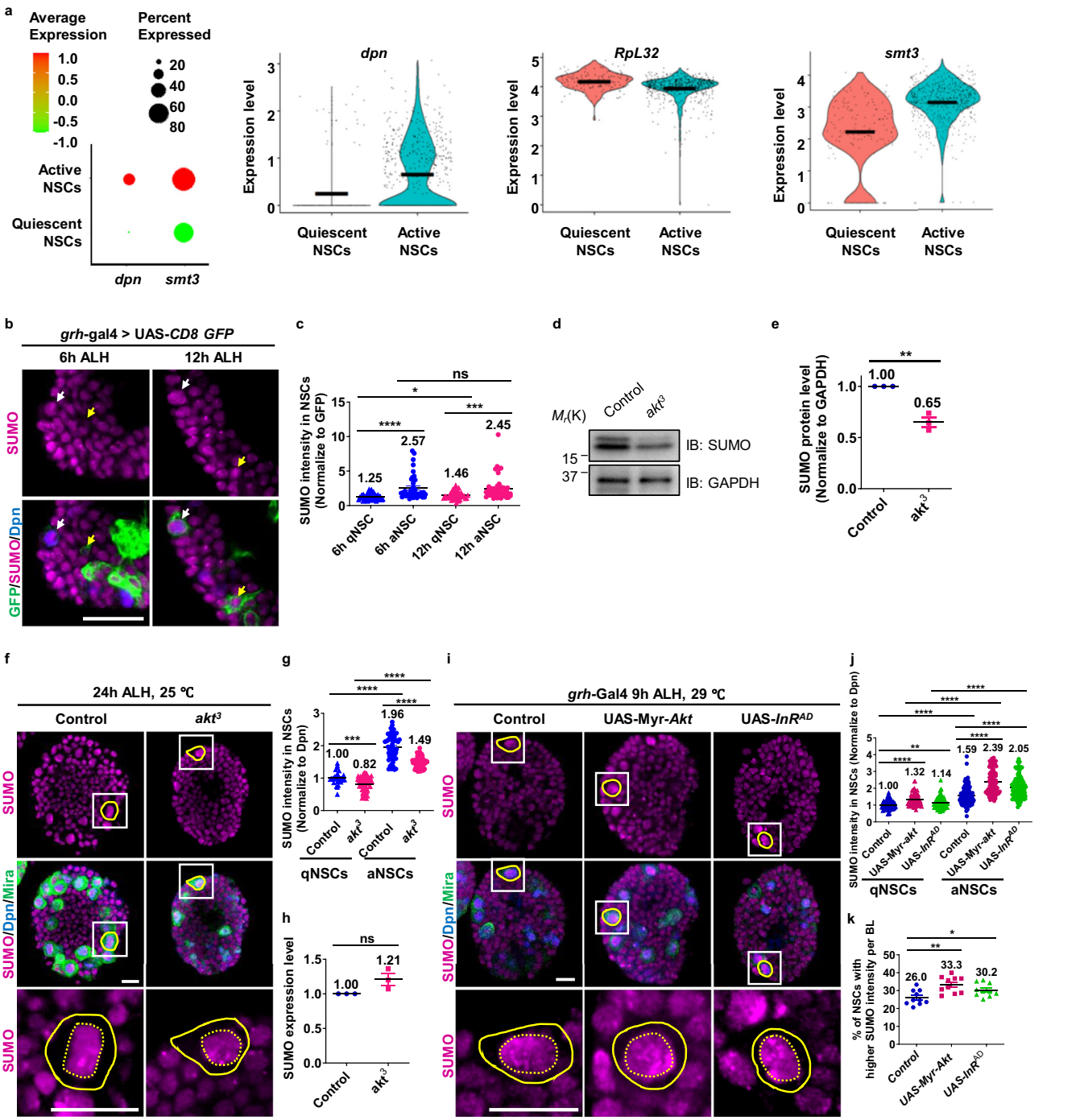

Fig. 3 | Akt stabilizes SUMO protein level during NSC reactivation. a Analysis of *smt3* and *dpn* mRNA expression in qNSCs and aNSCs from the dataset of single-cell RNA seq[62]. *RpL32* works as a house keeping gene. **b** Larval brains expressing mCD8-GFP driven by *grh*-GAL4. White arrows point to aNSCs. Yellow arrows point to qNSCs. **c** Quantification of SUMO intensity (normalized to GFP) at 6 h ALH for (**b**) in aNSCs (big Dpn+ cells) (2.57 ± 1.79, P = 4.4E-06, n = 10) and qNSCs (Dpn+ cells with protrusion) (1.25 ± 0.42, n = 10), at 12 h ALH in aNSCs (2.45 ± 1.66, P = 0.0003, P = 0.75, n = 10) and qNSCs (1.46 ± 0.57, P = 0.041, n = 10). **d** Fly brains from *yw* control and akt^3 at 24 h ALH were dissected to extract proteins for western blot. **e** Quantification of relative SUMO protein levels in (**d**), n = 3. Control, 1; akt^3, 0.65 ± 0.08, P = 0.002. At 24 h ALH (**f**) and 9 h ALH (**i**), larval brain lobes were labeled with SUMO, Dpn and Mira. The yellow circles labeled NSCs, lower panels are enlarged views of cells in white squares in upper panels, yellow dotted circles labeled the nucleus of NSCs. **g** Quantification of SUMO intensity (normalized to Dpn) in qNSCs and aNSCs in (**f**). QNSCs in control (*yw*), 1 ± 0.21, n = 10; qNSCs in akt^3, 0.82 ± 0.22, P = 0.0007, n = 10; aNSCs in control, 1.96 ± 0.38, P = 1.9E-20, n = 10; aNSCs in akt^3, 1.49 ± 0.17, P = 5.2E-38, P = 7.4E-15, n = 10. **h** Quantification of *smt3* mRNA fold enrichment in qPCR assay. At 24 h ALH, larva brains from *yw* control and akt^3 were dissected for qPCR, P = 0.07, n = 3. **i** Larval brain lobes from control (β-gal^{RNAi}), UAS-InR^{AD} and UAS-Myr-*Akt* lines driven by *grh*-Gal4. **j** Quantification graph of SUMO intensity (normalized to Dpn) in qNSCs and aNSCs in (**i**). qNSCs in control, 1 ± 0.26, n = 11; qNSCs in UAS-Myr-*Akt*, 1.32 ± 0.35, P = 2.1E-25, P = 7.8E-11, n = 10; qNSCs in UAS-InR^{AD}, 1.14 ± 0.33, P = 2.5E-08, P = 0.003, n = 10; aNSCs in control, 1.59 ± 0.56, P = 3.6E-17, n = 11; aNSCs in UAS-Myr-*Akt*, 2.39 ± 0.72, P = 4.1E-16, n = 10; aNSCs in UAS-InR^{AD}, 2.05 ± 0.63, P = 2.5E-08, n = 10. **k** Quantification of the % of NSCs with higher SUMO intensity per BL in (i). Control, 26 ± 11.8, n = 11; UAS-Myr-*Akt*, 33.3 ± 4.6, P = 0.001, n = 10; UAS-InR^{AD}, 30.2 ± 3.7, P = 0.027, n = 10. Yellow dotted circles labeled cell nucleus. Data are presented as mean ± SD. **** for P ≤ 0.0001, *** for P ≤ 0.001, ** for P ≤ 0.01, * for 0.05≤p ≤ 0.01, ns indicates p > 0.05. Scale bars: 10 μm.

https://doi.org/10.1038/s41467-024-52569-y

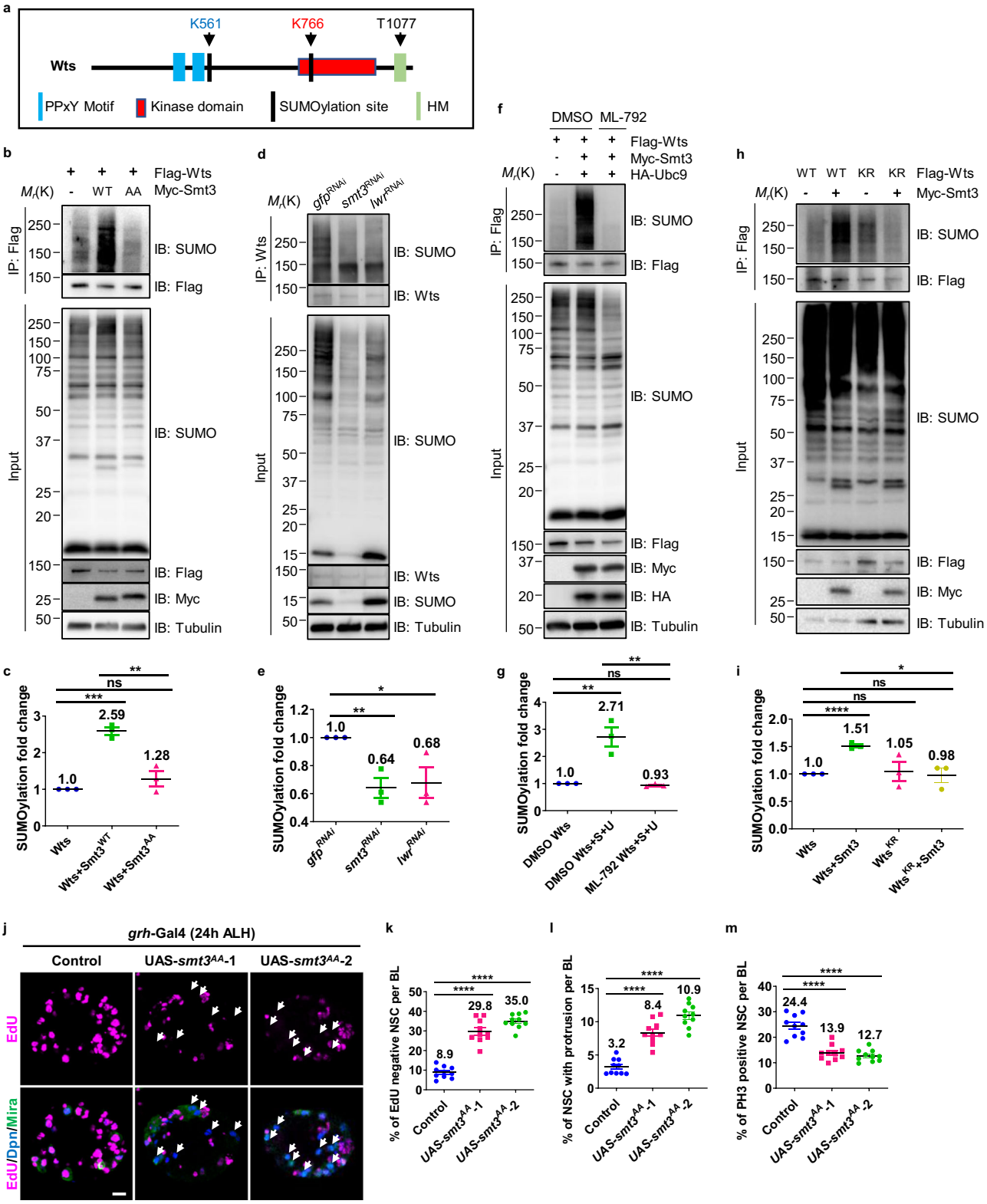

ML-792 is an effective inhibitor of SUMO activating enzyme (SAE, SUMO E1) that impedes the process of SUMOylation[69]. In the DMSO-treated control group within the IP samples, the overexpression of both Smt3 and Ubc9 substantially augmented Flag-Wts SUMOylation, with a 2.71-fold increase (Fig. 4f, g). However, when subjected to ML-792 inhibitor treatment, Flag-Wts SUMOylation was significantly reduced from 2.71-fold to 0.93-fold (Fig. 4f, g). This reduction is even more pronounced than the baseline level of SUMOylation observed without Smt3 and Ubc9 overexpression, which stands at 1-fold (Fig. 4f, g). Moreover, ML-792 inhibitor treatment also suppressed the overall SUMOylation in the input group (Fig. 4f). Furthermore, the SUMOylation of endogenous Wts in S2 cells is similarly disrupted by ML-792 inhibitor (Supplementary Fig 6b). Therefore, SUMO E1 enzyme is indispensable for facilitating Wts SUMOylation.

To determine whether Wts-K766 serves as the primary site for SUMOylation on Wts, the K766 residue in Wts was replaced with an

Fig. 4 | Wts is SUMOylated by Smt3 at Lys766. a The illustration of Wts protein. PPxY motif is required for Yki interaction. The SUMOylation site K766 is within the kinase domain of Wts protein. HM is hydrophobic motif, T1077 is the Thr phosphorylated by Hpo, and this site is within the hydrophobic motif of Wts protein. SUMOylation assays in S2 cells. IP was conducted with anti-Flag antibody (**b**, **f**, **h**) or anti-Wts antibody (**d**), and western blots were performed by using anti-SUMO and anti-Flag to detect SUMOylated Wts and overall levels of Flag-Wts, respectively. Tubulin serves as a loading control. **b** Flag-Wts and Myc-Smt3^{WT} or Myc-Smt3^{AA} were co-transfected into S2 cells. **d** S2 cells were treated with double stranded RNA against *gfp*, *smt3* or *lwr* for 72 h to induce knockdown. **f** Flag-Wts, Myc-Smt3 and HA-Ubc9 were co-transfected into S2 cells. 6 h before harvested, S2 cells were treated with DMSO or ML-792. **h** Flag-Wts^{WT} or Flag-Wts^{KR} was co-transfected with Myc-Smt3 into S2 cells. **c**, **e**, **g**, **i** Quantification of Wts SUMOylation for (**b**, **d**, **f**, **h**) respectively, n = 3. **c** Control (Flag-Wts), 1; Flag-Wts + Myc-Smt3^{WT}, 2.59 ± 0.18, P = 0.0001; Flag-Wts + Myc-Smt3^{AA}, 1.28 ± 0.35, P = 0.24, P = 0.005. **e** Control (*gfp*^{RNAi}), 1; *smt3*^{RNAi}, 0.64 ± 0.12, P = 0.007; *lwr*^{RNAi}, 0.68 ± 0.19, P = 0.004. **g** Control (Flag-Wts, DMSO), 1; Flag-Wts + Myc-Smt3 + HA-Ubc9 (DMSO), 2.71 ± 0.62, P = 0.009; Flag-Wts + Myc-Smt3 + HA-Ubc9 (ML-792), 0.93 ± 0.05, P = 0.07, P = 0.008. **i** Control (Flag-Wts^{WT}), 1; Flag-Wts^{WT} + Myc-Smt3, 1.51 ± 0.05, P = 7.4E-05; Flag-Wts^{KR}, 1.05 ± 0.29, P = 0.79; Flag-Wts^{KR} + Myc-Smt3, 0.98 ± 0.22, P = 0.87, P = 0.015. **j** At 24 h ALH, larval brain lobes from control (*β-gal*^{RNAi}) and UAS-*smt3*^{AA} lines driven by *grh*-Gal4 were analyzed for EdU incorporation. NSCs were marked by Dpn and Mira. White arrows point to EdU- qNSCs. **k** Quantification of EdU- NSCs per BL for (**j**). Control, 8.9 ± 3, n = 10; UAS-*smt3*^{AA}-1, 29.8 ± 5.8, P = 7.6E-09, n = 10; UAS-*smt3*^{AA}-2, 35 ± 3.6, P = 7.8E-13, n = 10. **l** Quantification of NSCs that retaining cellular protrusion per BL for (**j**). Control, 3.2 ± 1.2, n = 10; UAS-*smt3*^{AA}-1, 8.4 ± 1.8, P = 4.2E-07, n = 10; UAS-*smt3*^{AA}-2, 10.9 ± 1.7, P = 6.2E-10, n = 10. **m** Quantification of PH3+ NSCs per BL for (**j**). Control, 24.4 ± 4.3, n = 10; UAS-*smt3*^{AA}-1, 13.9 ± 3, P = 5.5E-06, n = 10; UAS-*smt3*^{AA}-2, 12.7 ± 2.3, P = 5.5E-07, n = 10. Data are presented as mean ± SD. **** for P ≤ 0.0001, ** for P ≤ 0.01, ∗ indicates 0.05≤p ≤ 0.01, ns indicates p > 0.05. Scale bars: 10 μm.

arginine (R) residue in the SUMOylation assay. In S2 cells, Myc-Smt3 overexpression led to a 1.5-fold increase in the SUMOylation of Flag-Wts, while the SUMOylation of Flag-Wts^{K776R} (Wts^{KR}) remained unchanged (Fig. 4h, i). This observation strongly suggests that K766 represents a major site of SUMOylation on Wts.

SUMO conjugation is required for NSC reactivation

We have generated transgenic flies expressing Venus-tagged conjugation-deficient SUMO (smt3^{AA}), verified its expression (Supplementary Fig 6c, d), and examined its effect on NSC reactivation. Notably, Venus-Smt3 localized to the nucleus (Supplementary Fig 1l, 6e), while Venus-Smt3^{AA} localized to both cytoplasm and nucleus of the NSCs (Supplementary Fig 6c, e), consistent with a previous report[37]. Interestingly, at 24 h ALH, overexpression of *smt3*^{AA} led to NSC reactivation defects, with a significant increase in the percentage of NSCs lacking EdU incorporation (Fig. 4j, k, 8.9% in the control; 29.8% and 35% in the *smt3*^{AA} lines). Additionally, the percentage of NSCs retaining their cellular protrusion significantly increased from 3.2% in control to 8.4% and 10.9% in *smt3*^{AA} lines (Fig. 4l). Furthermore, there was a significant decrease in the percentage of PH3-positive NSCs in *smt3*^{AA} mutant brains (13.9% and 12.7%) compared to control (24.4%; Fig. 4m). These findings suggest that SUMO relies on its conjugation activity to regulate NSC reactivation.

SUMOylation of Wts at Lys766 attenuates its phosphorylation and kinase activity in vitro

The phosphorylation level of Wts-Thr1077 (p-Wts) by Hpo kinase is the principal readout of the Hippo pathway activity[70]. We examined p-Wts levels in S2 cells, wherein we expressed Flag-Wts or Flag-Wts^{KR}, both with and without co-expression of Myc-Hpo. As expected, Hpo overexpression significantly increased Wts phosphorylation on Thr1077 from 0.57-fold to 1-fold (Fig. 5a, b, first 2 lanes). Even without *hpo* overexpression, the phosphorylation level of Wts^{KR} by Hpo well exceeded that of wild-type Wts (Fig. 5a, b, lane 3 vs lane 1, 0.96-fold vs 0.57-fold), and with *hpo* co-overexpression, Wts^{KR} phosphorylation level remained notably higher than that of wild-type Wts (Fig. 5a, b, lane 4 vs lane 2, 2.25-fold vs 1-fold). These observations suggest that the SUMOylation deficient Wts has higher phosphorylation level than wild-type Wts.

hpo knockdown in S2 cells significantly reduced the phosphorylation levels of Wts^{KR} from 2.25-fold to 1.12-fold (Fig. 5c, d, lane 3 vs lane 4; Supplementary Fig 7a), suggesting that either Hpo kinase exhibits a preference for phosphorylating SUMOylation-deficient Wts or phosphorylation of non-SUMOylated Wts is stabilized.

To distinguish between these two possibilities, we conducted cycloheximide (CHX) chase assays in S2 cells to block protein biosynthesis and detect Wts or Wts^{KR} protein levels in a time-course experiment. Notably, the phosphorylation level of wild-type Wts remained relatively stable (from 1-fold to 1.17-fold), albeit much lower than Wts^{KR} (Fig. 5e, f), whereas the phosphorylated Wts^{KR} decreased slightly from 1.82-fold to 1.55-fold within 6 h in the IP group (Fig. 5e, f). This finding suggests that phosphorylation of non-SUMOylated Wts did not result in its stabilization. Therefore, we favor the model that Hpo kinase preferentially phosphorylates SUMOylation-deficient Wts than the wild-type Wts.

Upon its phosphorylation by Hpo kinase, Wts further phosphorylates Yki primarily at Ser168 (p-Yki), leading to its cytoplasmic retention and inactivation[23,70,71]. In S2 cells, co-expression of Flag-Wts with HA-Yki resulted in a slight increase in Yki phosphorylation from 0.7-fold to 1-fold (Fig. 5g, h). Notably, co-expression of Flag-Wts^{KR} further increased Yki phosphorylation to 2.07-fold (1.83-fold after further normalized to Flag-Wts protein levels, Fig. 5g, i). Moreover, in input group, Yki band exhibited a slight upward shift when co-expressed with wild-type *wts*, and a more pronounced upward shift (implying Yki phosphorylation) when co-expressed with *wts*^{KR} (Fig. 5g). This observation confirms that the SUMOylation-deficient mutant Wts^{KR} functions as an active form of Wts, exhibiting a higher kinase activity towards Yki than wild-type Wts.

Treatment of a SUMOylation inhibitor, ML-792, significantly reduced Wts SUMOylation to 0.58-fold (Fig. 5j, k), compared to untreated cells. Meanwhile, the phosphorylation levels of Wts and Yki increased 2.35- and 2.42-folds, respectively, as compared to control cells (Fig. 5j, l, m). Our data suggests that Wts SUMOylation at K766 diminishes its kinase activity, thereby reducing p-Yki levels to allow NSC reactivation.

SUMOylation-deficient mutant of Wts (Wts^{KR}) represents a hyperactive form of Wts in vivo

We generated transgenic flies expressing Venus-tagged Wts^{KR} and verified them by immunostaining (Supplementary Fig 7b, c). Importantly, wild-type Wts and Wts^{KR} strains had similar Wts protein levels in NSCs (Supplementary Fig 7b, c). Similar to previous reports that overexpression of wild-type *wts* resulted in NSC reactivation defects[20,22,26], we observed that 23.2% of Wts-overexpressing NSCs failed to incorporate EdU, compared with 6.7% in control (Fig. 6a, b). Remarkably, two independent *wts*^{KR}-overexpressing NSC lines showed a more severe defect, with 39.7% and 34.4% of these NSCs remaining without EdU incorporation (Fig. 6a, b). Additionally, there were more NSCs exhibiting primary cellular protrusions, with percentage increased from 3.3% in control to 6.7% in wild-type *wts* overexpression line, to 11.9% and 10.2% in *wts*^{KR} overexpression lines (Fig. 6c). Conversely, the percentage of PH3-positive NSCs decreased to 12% and 14.9% in *wts*^{KR} overexpressing lines, compared to 24.4% in control, 17.5% in wild-type *wts*-overexpressing line, (Fig. 6d).

Consistent with our data in S2 cells, *wts*^{KR} overexpression in larval brains had a similar effect on the phosphorylation levels of

https://doi.org/10.1038/s41467-024-52569-y

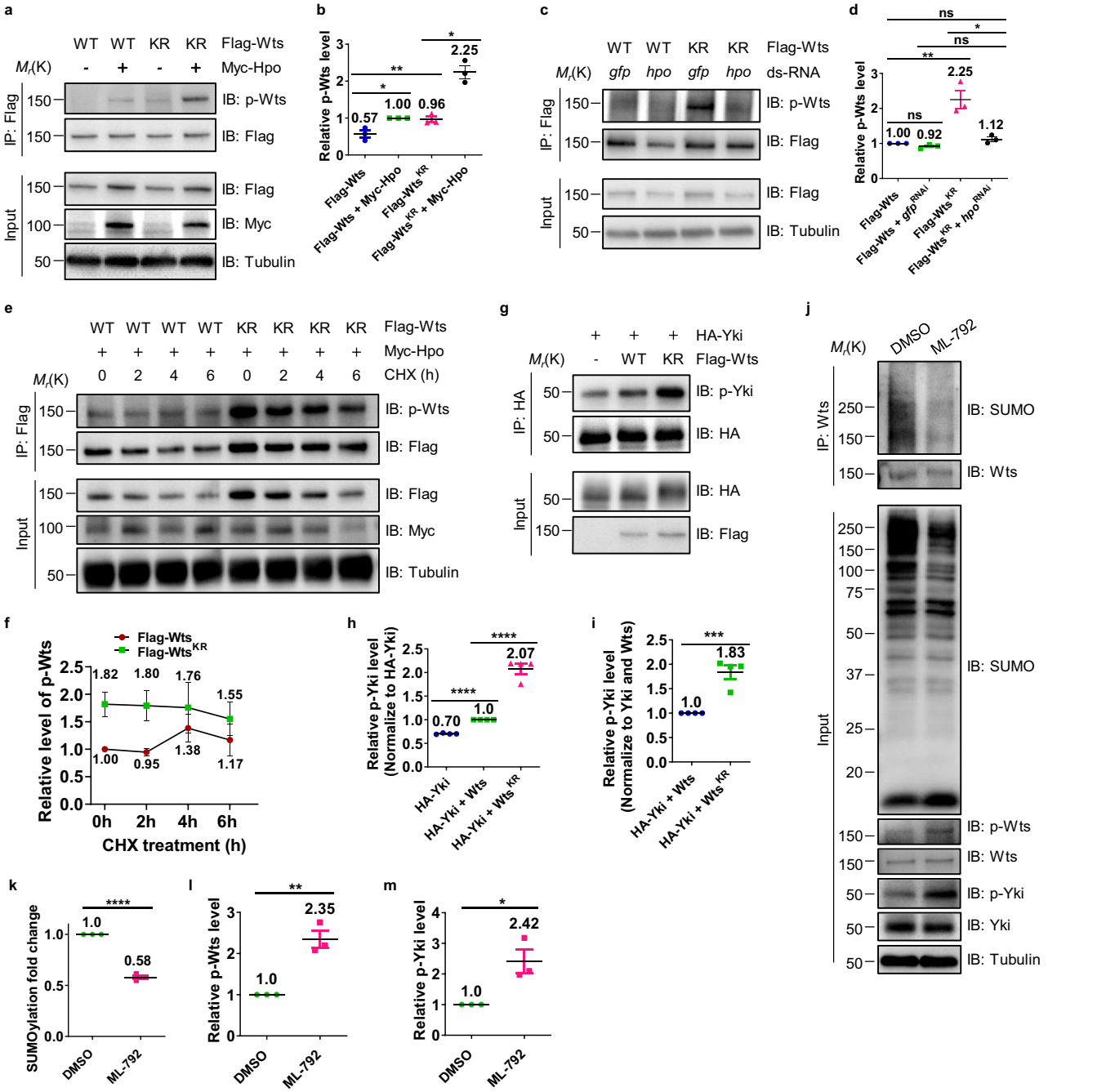

Fig. 5 | SUMOylation of Wts at Lys766 suppresses its phosphorylation and attenuates its kinase activity. a, **c**, **e**, **g**, **j** S2 cells transfected with various constructs or with indicated treatment were collected for IP followed by Western blotting. **b**, **d**, **f**, **h**, **i**, **k**–**m** Quantification of the indicated protein levels or fold changes in (**a**, **c**, **e**, **g**, **j**) respectively, from three-four independent repeats. **b**, **d** Relative p-Wts levels (normalize to Flag-Wts or Flag-Wts^{KD}) in (**a**, **c**). **b** Control (Flag-Wts), 0.57 ± 0.17, P = 0.012; Flag-Wts + Myc-Hpo, 1; Flag-Wts^{KR}, 0.96 ± 0.13, P = 0.036; Flag-Wts^{KR} + Myc-Hpo, 2.25 ± 0.3, P = 0.002, P = 0.30. **d** Control (Flag-Wts + *gfp*^{RNAi}), 1; Flag-Wts + *hpo*^{RNAi}, 0.92 ± 0.05, P = 0.07, P = 0.054; Flag-Wts^{KR} + *gfp*^{RNAi} 2.25 ± 0.45, P = 0.008; Flag-Wts^{KR} + *hpo*^{RNAi}, 1.12 ± 0.11, P = 0.15, P = 0.013. **e** S2 cells were treated with cycloheximide (CHX) prior to IP. **f** Relative level of p-Wts for (**e**) (p-Wts normalized to Flag-Wts$^{(KR)}$). Wts^{WT} 0 h: 1, 2 h: 0.95 ± 0.07; 4 h: 1.38 ± 0.26; 6 h: 1.17 ± 0.29; Wts^{KR} 0 h: 1.82 ± 0.22, 2 h: 1.79 ± 0.27; 4 h: 1.76 ± 0.45; 6 h: 1.55 ± 0.3. **g** Yki and p-Yki are detected in S2 cells transfected with various constructs. **h** Relative p-Yki levels in (**g**). Control (HA-Yki), 0.7 ± 0.01, P = 6.6E-09; HA-Yki + Flag-Wts, 1; HA-Yki + Flag-Wts^{KR} 2.07 ± 0.22, P = 5.9E-05. **i** Quantification of relative p-Yki levels, which was first normalized to HA-Yki and then further normalized to Flag-Wts from four repeats in (**g**). HA-Yki + Flag-Wts, 1; HA-Yki + Flag-Wts^{KR} 1.83 ± 0.28, P = 0.0009. **j** S2 cells transfected with various constructs were treated with DMSO or ML-792. Wts, p-Wts, Yki, and p-Yki were detected following IP. **k**–**m** Quantifications for (**j**). **k** Wts SUMOylation fold change. DMSO, 1; ML-792, 0.58 ± 0.03, P = 2.2E-05. **l** Relative p-Wts level. DMSO, 1; ML-792, 2.35 ± 0.36, P = 0.003. **m** p-Yki level. DMSO, 1; ML-792, 2.42 ± 0.66, P = 0.02. Data are presented as mean ± SD. ns indicates p ≥ 0.05; * indicates 0.05≤ p ≤ 0.01, ** indicates p ≤ 0.01, **** indicates p ≤ 0.0001. Scale bars: 10 μm.

endogenous Wts and Yki (Fig. 6e–g). At 24 h ALH, larval brains overexpressing wild-type *wts* under *actin*-gal4 (*act*-gal4), exhibited a slight increase in Wts phosphorylation levels (1.25-fold) and Yki (1.48-fold) phosphorylation levels compared to control brains (1-fold, Fig. 6e–g). Remarkably, larval brains overexpressing *wts*^{KR} displayed a significantly higher increase in Wts phosphorylation levels (2.33-fold) and Yki (3.04-fold) phosphorylation levels (Fig. 6e–g). These in vivo findings confirmed that SUMOylation-deficient mutant of Wts (wts^{KR}) is a hyperactive form of Wts.

https://doi.org/10.1038/s41467-024-52569-y

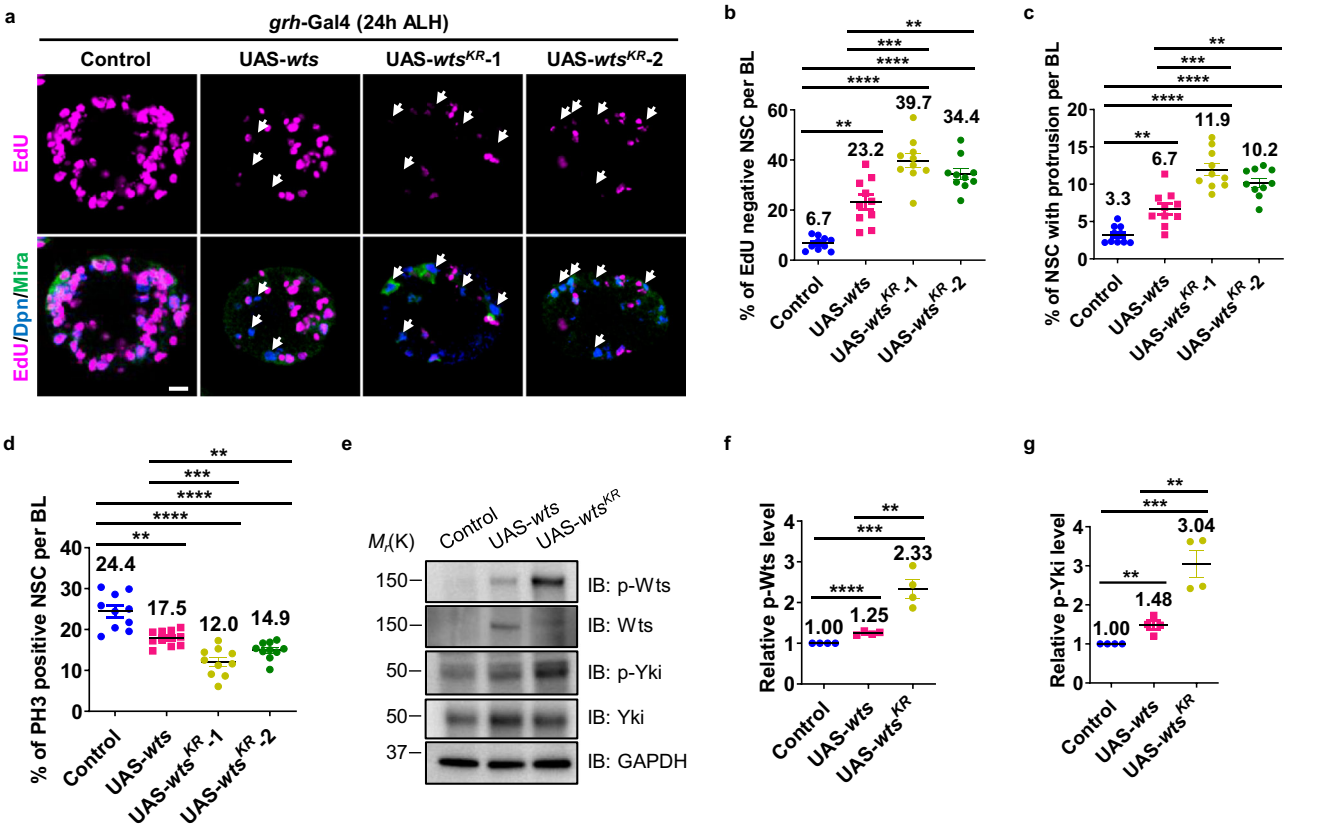

Fig. 6 | Wts SUMOylation deficient mutant functions as an active form of Wts kinase to suppress NSC reactivation. a At 24 h ALH, larval brain lobes from control (β-gal^{RNAi}), UAS-*wts* and UAS-wts^{KR} driven by *grh*-Gal4 were analyzed for EdU incorporation. NSCs were marked by Dpn and Mira. White arrows point to EdU^- qNSCs. **b** Quantification of EdU^- NSCs per BL for (**a**). Control, 6.7 ± 2.6, n = 10; UAS-*wts*, 23.2 ± 9.1, P = 0.0012, n = 10; UAS-wts^{KR}–1, 39.7 ± 8.9, P = 1.4E-09, P = 0.0007, n = 10; UAS-wts^{KR}-2, 34.4 ± 6.7, P = 4.5E−10, P = 0.0059, n = 10. **c** Quantification of NSCs retaining cellular protrusion per BL for (**a**). Control, 3.3 ± 1.2, n = 10; UAS-*wts*, 6.7 ± 2.3, P = 0.0005, n = 10; UAS-wts^{KR}–1, 11.9 ± 2.6, P = 1.2E-08, P = 0.00014, n = 10; UAS-wts^{KR}–2, 10.2 ± 1.9, P = 7.9E-09, P = 0.0014, n = 10. **d** Quantification of PH3+ NSCs per BL for (**a**). Control, 24.4 ± 4.3, n = 10; UAS-*wts*, 17.5 ± 1.9, P = 0.007, n = 10; UAS-wts^{KR}-1, 12 ± 3.4, P = 0.0002, n = 10; UAS-wts^{KR}–2, 14.9 ± 2.1, P = 6.8E-06, n = 10. **e** Proteins were extracted from larval brains of control (β-gal^{RNAi}), UAS-*wts* and UAS-wts^{KR} driven by *actin*-Gal4 for Western blot. **f**, **g** Quantification of four independent repeats in (**e**). **f** Control 1; UAS-*wts*, 1.25 ± 0.05, P = 3.4E-05; UAS-wts^{KR} 2.33 ± 0.45, P = 0.0009, P = 0.003. **g** Control, 1; UAS-*wts*, 1.48 ± 0.22, P = 0.005; UAS-wts^{KR} 3.04 ± 0.68, P = 0.001, P = 0.005. Data are presented as mean ± SD. * indicates 0.05≤ p ≤ 0.01, ** indicates p ≤ 0.01, *** indicates p ≤ 0.001, **** indicates p ≤ 0.0001. Scale bars: 10 μm.

SUMOylation of Wts promotes Yki nuclear localization in NSCs

At 24 h ALH, Yki predominantly localized within the nucleus of NSCs in control larval brains. Interestingly, the percentage of nuclear Yki (nYki) significantly reduced to 13.5% in *smt3* and 31.8% in *lwr* mutant NSCs (Fig. 7a, b) as compared to 90.8% in control NSCs. Furthermore, the intensity of nYki in NSCs dramatically decreased from 1-fold in control NSCs to 0.5-fold and 0.59-fold in *smt3*- and *lwr*-mutant NSCs, respectively (Fig. 7a, c). These observations suggest that the Hippo pathway is activated upon depletion of SUMOylation pathway components. Moreover, overexpression of the SUMO-deficient mutant $smt3^{4A}$ in NSCs at 24 h ALH also significantly inhibited nuclear localization of Yki (69% and 64.9% in $smt3^{4A}$ lines compared to 88.2% in control; Fig. 7d, e), with a significant reduction in nYki intensity in NSCs (Control, 1-fold; $smt3^{4A}$ lines, 0.61-fold and 0.61-fold; Fig. 7d, f). At 24 h ALH, overexpression of wild-type *wts* in NSCs led to a minor reduction in the percentage of NSCs with nYki: 87.1% in control vs 60.5% in *wts*-overexpressing NSCs, and in nYki intensity: 1-fold in control vs 0.79-fold in *wts*-overexpressing NSCs (Fig. 7g–i). However, overexpression of wts^{KR} in NSCs resulted in a more dramatic decrease in the percentage of nYki NSCs (20.5%) and nYki intensity (0.49-fold) (Fig. 7g–i). These data suggest that the SUMO pathway-dependent downregulation of the Hippo pathway promotes the nuclear localization of Yki, and consequently, NSC reactivation.

SUMOylation of Wts promotes the expression of Yki target genes in NSCs

We re-analyzed gene expression data from the single-cell RNA sequencing dataset[62] and found the expression patterns for *diap1* and *cycE*, potential targets of Yki, to be similar to that of *smt3* and *lwr*—exhibiting significantly higher expression levels in the active NSCs compared to quiescent NSCs (Supplementary Fig 8a). Moreover, loss of *smt3* or *lwr* function led to a substantial decrease in CycE protein intensity in NSCs from 1-fold to 0.33-fold in *smt3* mutant and 0.36-fold in *lwr* mutant NSCs (Fig. 7j, k). Furthermore, *smt3* knockdown in NSCs also resulted in a noticeable reduction in CycE protein levels (Supplementary Fig 8b, c). The intensity of CycE protein and Ban-lacZ also decreased in these NSCs, with a more pronounced reduction in wts^{KR}-overexpressing NSCs (Fig. 7l, m and Fig. 7n, o). These data further support that the SUMO pathway downregulates the Hippo pathway to allow Yki to function for NSC reactivation.

The SUMO pathway downregulates Wts protein levels in vitro

We test whether SUMOylation of Wts is responsible for the downregulation of Wts protein levels. Indeed, the western blots showed that SUMO and Ubc9 downregulated Wts protein levels in a dosage-dependent manner in S2 cells (Fig. 8a–d). Moreover, in CHX chase assays, Smt3- and Ubc9-overexpression accelerates, the rate of Wts protein degradation, compared to control conditions without Smt3

https://doi.org/10.1038/s41467-024-52569-y

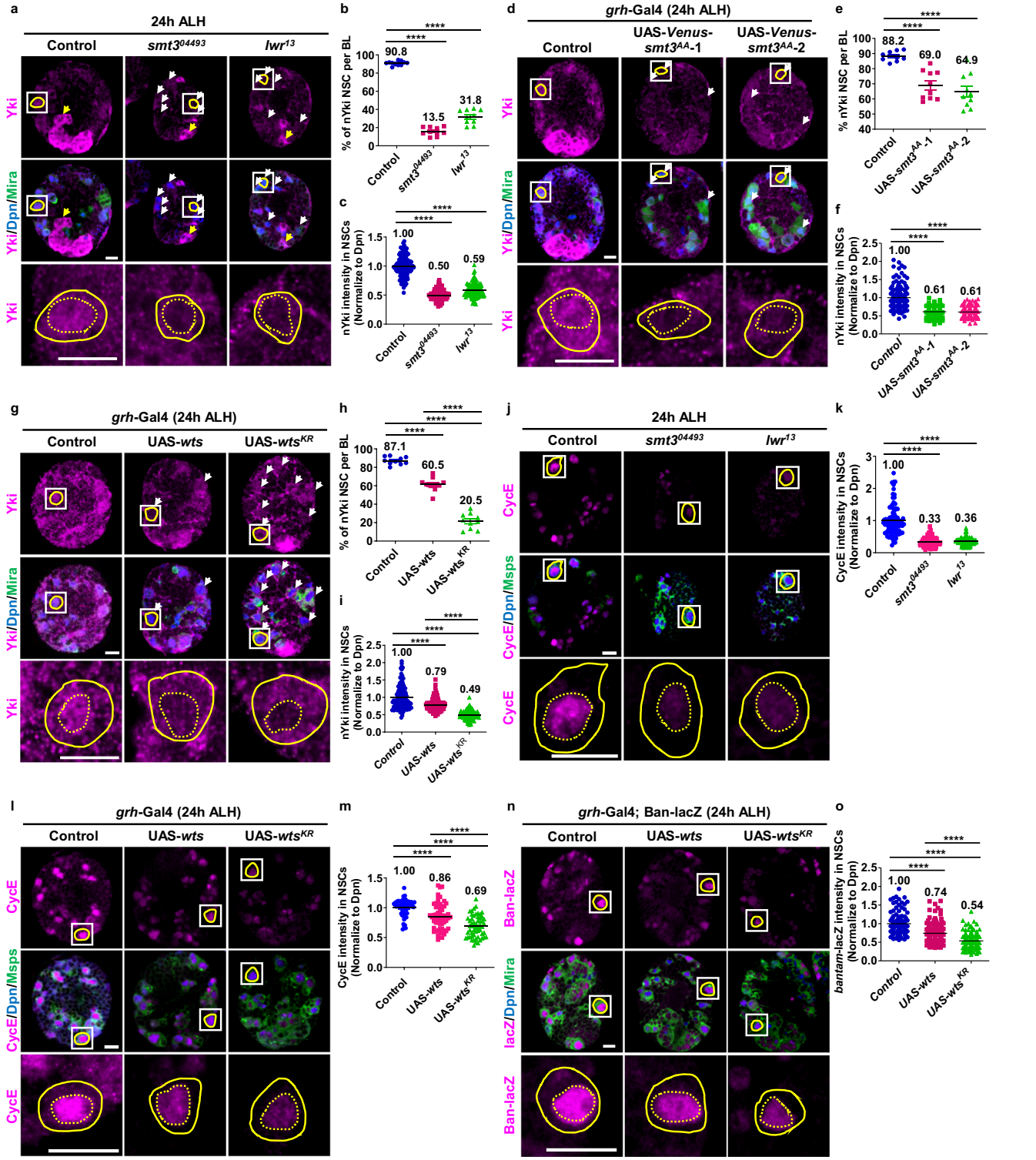

and Ubc9 overexpression (Fig. 8e, f). By contrast, Wts degradation is abrogated by *smt3*^{AA} overexpression (Fig. 8g, h), suggesting that Wts degradation requires the SUMO conjugation activity of Smt3.

The SUMO pathway downregulates Wts protein levels in vivo

Next, we investigated whether the SUMOylation pathway regulates Wts protein levels in larval brains. Notably, we observed that Wts intensity increased significantly in *smt3*^{04493} and *lwr*^{13} mutants in both quiescent NSCs (Fig. 9a, b; 1.34-fold and 1.23-fold vs 1-fold in control) and active NSCs (1.58-fold and 1.5-fold vs 1.22-fold in control). Conversely, Wts protein intensity decreased significantly from 1-fold in control to 0.84-fold and 0.75-fold in two *smt3* overexpression lines (Fig. 9c, d) and to 0.81-fold in *lwr* overexpression line (Fig. 9g, h). Intriguingly, Wts intensity in NSCs is significantly increased when conjugation-deficient SUMO (*smt3*^{AA}) or dominant-negative *lwr* (*lwr*^{DN}) was overexpressed (1.52-fold and 1.6-fold in *smt3*^{AA} overexpression lines, Fig. 9e, f; and 1.25-fold in *lwr*^{DN} overexpression line, Fig. 9g, h) as compared to control. Quantitative real-time PCR results showed that *wts* mRNA levels had no significant difference in *smt3* or *lwr* mutant larval brains, compare to the control (Fig. 9i), suggesting a regulation independent of gene expression.

https://doi.org/10.1038/s41467-024-52569-y

Fig. 7 | Wts SUMOylation promotes Yki nuclear localization and Yki target genes expression in NSCs. a, **d**, **g**, **j**, **l**, **n** At 24 h ALH, larval brain lobes were labeled with indicated proteins. NSCs were marked by Dpn and Mira or Msps. **a**, **d**, **g** White arrows point to NSCs without nYki localization. The Yki^{+} Dpn^{-} cells pointed by yellow arrows are optic lobe cells. **b**, **e**, **h** Quantification of NSCs with nYki per BL in (**a**, **d**, **g**) respectively. **b** Control (*yw*), 90.8 ± 2.3, n = 11; *smt3*^{O4493}, 13.5 ± 4.6, P = 2.8E −21, n = 12; *lwr*^{13}, 31.8 ± 7.8, P = 5.0E-13, n = 10. **e** Control (*β-gal*^{RNAi}), 88.2 ± 3.1, n = 10; UAS-*smt3*^{4A}-1, 69 ± 9.5, P = 9.7E-06, n = 10; UAS-*smt3*^{4A}-2, 65 ± 11.1, P = 5.0E-06, n = 10. **h** Control (*β-gal*^{RNAi}), 87.1 ± 4.2, n = 10; UAS-*wts*, 60.5 ± 7.3, P = 1.6E-08, n = 10; UAS-*wts*^{KR}, 20.5 ± 8.5, P = 2.0E-14, P = 1.5E-09, n = 10. **c**, **f**, **i** Quantification of nYki intensity (normalized to Dpn) in NSCs in (**a**, **d**, **g**) respectively. (**c**) Control, 1 ± 0.18, n = 11; *smt3*^{O4493}, 0.5 ± 0.09, P = 4.0E-82, n = 12; *lwr*^{13}, 0.59 ± 0.12, P = 1.9E-56, n = 10. **f** Control (*β-gal*^{RNAi}), 1 ± 0.35, n = 10; UAS-*smt3*^{4A}-1, 0.61 ± 0.14, P = 2.4E-27, n = 10; UAS-*smt3*^{4A}-2, 0.61 ± 0.15, P = 7.3E-23, n = 10. **i** Control (*β-gal*^{RNAi}), 1 ± 0.35, n = 10; UAS-*wts*, 0.79 ± 0.18, P = 4.6E-09, n = 10; UAS-*wts*^{KR}, 0.49 ± 0.12, P = 4.3E-42, P = 1.8E-42, n = 10. **k**, **m** Quantification of CycE intensity (normalized to Dpn) in NSCs in (**j**, **l**) respectively. **k** Control (*yw*), 1 ± 0.47, n = 10; *smt3*^{O4493}, 0.33 ± 0.13, P = 4.1E-37, n = 15; *lwr*^{13}, 0.36 ± 0.11, P = 4.3E-29, n = 13. **m** control (*β-gal*^{RNAi}), 1 ± 0.14, n = 10; UAS-*wts*, 0.86 ± 0.22, P = 8.7E-05, n = 10; UAS-*wts*^{KR}, 0.69 ± 0.18, P = 3.2E-17, P = 2.1E-05, n = 10. **n** Larval brain lobes from control (*β-gal*^{RNAi}), UAS-*wts* and UAS-*wts*^{KR} lines driven by *grh*-Gal4; Ban-lacZ were labeled with Dpn, Msps, and β-gal (Ban-lacZ). **o** Quantification of Ban-lacZ intensity (normalized to Dpn) in NSCs in (**n**). Control, 1 ± 0.28, n = 10; UAS-*wts*, 0.74 ± 0.26, P = 1.6E-13, n = 13; UAS-*wts*^{KR}, 0.54 ± 0.2, P = 2.3E-13, P = 4.0E-41, n = 14. The yellow circles labeled the NSCs, the lower panels are enlarged views of the cells in the white squares in the upper panels, the yellow dotted circles labeled the nucleus of the NSCs. Data are presented as mean ± SD. ** for P ≤ 0.01, **** for P ≤ 0.0001. Scale bars: 10 μm.

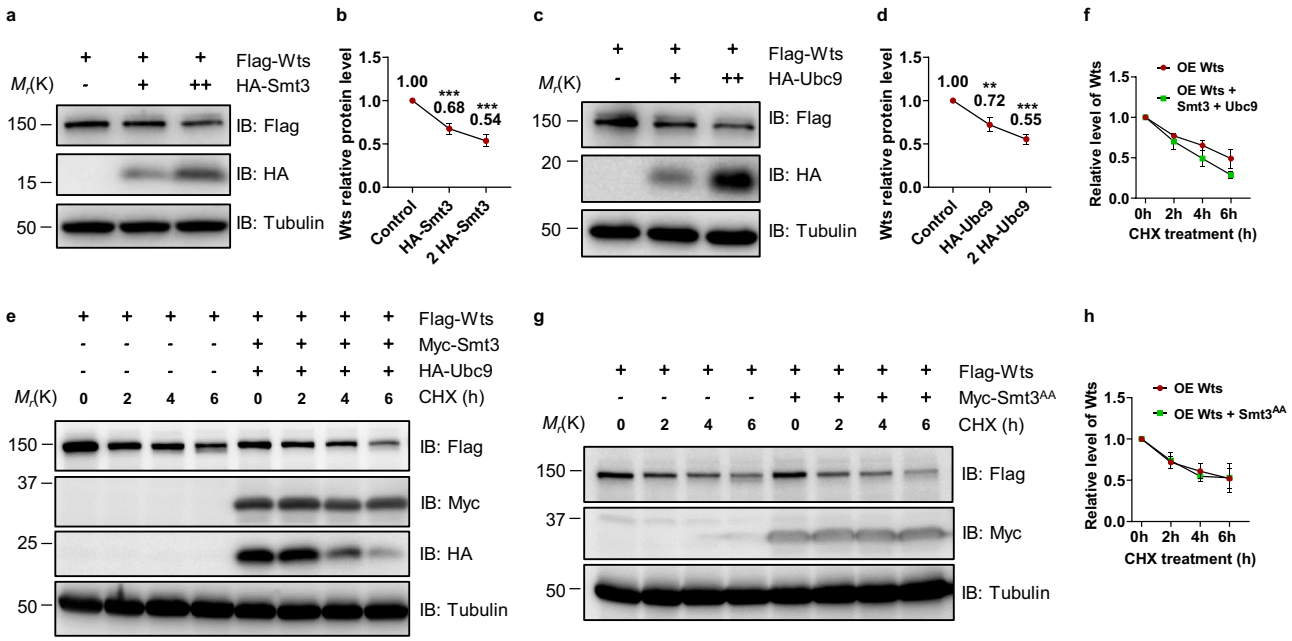

Fig. 8 | The SUMO pathway downregulates Wts protein level in vitro. **a**, **c** Western blotting in S2 cells expressing indicated proteins. **e**, **g** S2 Cells expressing indicated proteins were treated with cycloheximide (CHX) for indicated intervals and collected for Western blotting with indicated antibodies. **b**, **d**, **f**, **h** Quantification of Wts protein levels for (**a**, **c**, **e**, **g**) respectively (normalized to Tubulin). Data here is the mean of 3 independent experiments. **b** Flag-Wts, 1; Flag-Wts+HA-Smt3, 0.68 ± 0.06, P = 0.0007; Flag-Wts+2 HA-Smt3, 0.54 ± 0.07, P = 0.0003. **d** Flag-Wts, 1; Flag-Wts+HA-Ubc9, 0.72 ± 0.08, P = 0.004; Flag-Wts+2 HA-Ubc9, 0.55 ± 0.06, P = 0.0002. Flag-Wts, 0 h, 1; 2 h, 0.77 ± 0.02; 4 h, 0.65 ± 0.07; 6 h, 0.49 ± 0.12; Flag-Wts+Myc-Smt3, 0 h, 1; 2 h, 0.7 ± 0.1; 4 h, 0.49 ± 0.1; 6 h, 0.29 ± 0.04; (**f**) Flag-Wts, 0 h, 1; 2 h, 0.72 ± 0.07; 4 h, 0.61 ± 0.09; 6 h, 0.52 ± 0.12; Flag-Wts+Myc-Smt3^{AA}, 0 h, 1; 2 h, 0.74 ± 0.1; 4 h, 0.55 ± 0.06; 6 h, 0.53 ± 0.18. Data are presented as mean ± SD. *** for 0.001 ≤ P ≤ 0.0001, ** for 0.01 ≤ P ≤ 0.001.

We analyzed *wts*^{Venus}, in which a Venus-tagged *wts* was expressed under its endogenous promoter[72]. The localization pattern of *wts*^{Venus} by anti-GFP (Venus) staining was similar to that of anti-Wts antibody staining in the larval brain but with brighter signal (Supplementary Fig 9a). Consistent with the results obtained by anti-Wts antibody staining, loss of function of *smt3* led to a significant increase in Wts^{Venus} intensity (Supplementary Fig 9b–d). Moreover, overexpression of wild type *lwr* resulted in a decrease in Wts^{Venus} intensity (0.89-fold), while overexpression of dominant negative *lwr*^{DN} resulted in an increase in Wts^{Venus} intensity (1.2-fold) (Supplementary Fig 9e, f). These findings suggest that Smt3 and Ubc9 play a pivotal role in promoting Wts SUMOylation, subsequently leading to Wts protein degradation during NSC reactivation.

At 96 h ALH, *lwr*^{13} optic lobes were much smaller compared to control brains, with the total number of Dpn+ cells in *lwr*^{13} optic lobes being significantly lower than that in control (41.9 vs 223.2 in control, Supplementary Fig 9g, h). In addition, 46.8% of Dpn+ cells in *lwr*^{13} optic lobes were EdU-negative, while all Dpn+ cells in the control optic lobes were EdU-positive (Supplementary Fig 9g, i). In addition, Wts intensity in Dpn+ cells in *lwr*^{13} optic lobes was significantly higher than that in control optic lobes (1.41-fold, Supplementary Fig 9j, k). Thus, SUMOylation may also regulate Wts in other cell types.

Wts predominantly localizes in the cytoplasm but is also present in the nucleus in NSCs (Supplementary Fig 9a, b). Given that Smt3 localizes to the nucleus (Supplementary Figs 1l, 6e), it is likely that Wts is SUMOylated in the nucleus. This is consistent with the findings that most SUMO substrates are localized in the nucleus[73] and that CRL4-mediated inhibition of the hippo pathway kinases Lats1/2 occurs in the nucleus[74].

SUMO pathway promotes NSC reactivation by inhibiting the Hippo pathway

Simultaneous loss of *smt3* and *wts* by RNAi significantly suppressed the EdU-negative phenotype seen in *smt3*-depleted brains alone (Fig. 10a, b; *smt3*^{RNAi} = 54.3%. *smt3*^{RNAi}; *wts*^{RNAi} = 28.6%), while *wts*^{RNAi} brains showed no reactivation defects (Fig. 10a, b; 9.2%). Similarly, at 24 h ALH, the number of EdU-negative NSCs in brains depleted of both *lwr* and *wts* dramatically reduced to 37.8% compared with 65.7% in *lwr*^{13}

https://doi.org/10.1038/s41467-024-52569-y

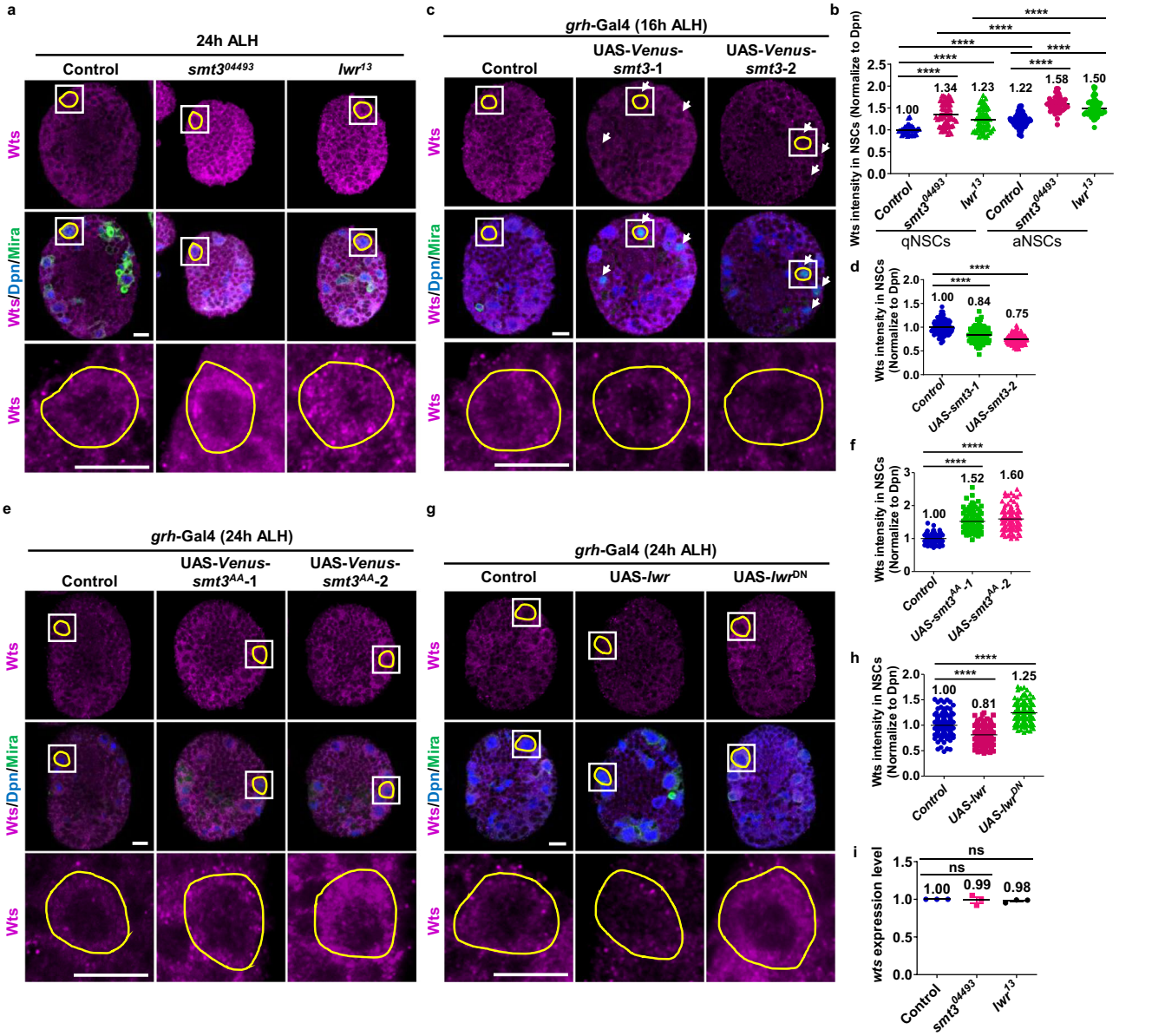

Fig. 9 | The SUMO pathway downregulates Wts protein level in vivo. At 24 h ALH (**a**, **e**, **g**) or 16 h ALH (**c**), larval brain lobes from indicated genotypes were labeled with Wts, Dpn and Mira, Venus tag in (**c**) and (**e**) also showed expression in NSCs. The yellow dotted circles labeled the Dpn+ and Mira+ NSCs; white arrows pointed to Venus positive NSCs. The lower panels are enlarged views of the cells in yellow dotted circles in upper panels. **b**, **d**, **f**, **h** Quantification of Wts intensity in NSCs normalized to Dpn in various genotypes in (**a**, **c**, **e**, **g**) respectively. **b**, qNSCs in control (*yw*), 1 ± 0.1, n = 12; qNSCs in *smt3*^{O4493}, 1.34 ± 0.26, P = 4.2E-11, n = 11; qNSCs in *lwr*^{13}, 1.23 ± 0.25, P = 1.3E-06, n = 10; aNSCs in control, 1.22 ± 0.14, P = 1.6E-14, n = 12; aNSCs in *smt3*^{O4493}, 1.58 ± 0.17, P = 1.0E-30, P = 1.3E-07, n = 11; aNSCs in *lwr*^{13}, 1.5 ± 0.19, P = 3.5E-20, P = 5.4E-09, n = 10. **d** Control (*β-gal*^{RNAi}), 1 ± 0.14, n = 13; UAS-*smt3*-1, 0.84 ± 0.16, P = 3.6E-18, n = 11; UAS-*smt3*-2, 0.75 ± 0.1, P = 1.2E-45, n = 11. **f** Control (*β-gal*^{RNAi}), 1 ± 0.12, n = 12; UAS-*smt3*^{4A}-1, 1.52 ± 0.28, P = 1.2E-51, n = 10; UAS-*smt3*^{4A}-2, 1.6 ± 0.34, P = 5.1E-49, n = 10. **h** Control (*β-gal*^{RNAi}), 1 ± 0.2, n = 10; UAS-*lwr*, 0.81 ± 0.18, P = 1.4E-14, n = 10; UAS-*lwr*^{DN}, 1.25 ± 0.2, P = 5.0E-21, n = 10. **i** Quantification of *wts* mRNA fold enrichment in qPCR assay. At 24 h ALH, larval brains from control (*yw*), *smt3*^{O4493} and *lwr*^{13} were dissected for qPCR, n = 3. Control, 1; *smt3*^{O4493}, 0.99 ± 0.07, P = 0.82; *lwr*^{13}, 0.98 ± 0.02, P = 0.15. The yellow circles labeled the NSCs, the lower panels are enlarged views of the cells in the white squares in the upper panels. Data are presented as mean ± SD. **** for P ≤ 0.0001. Scale bars: 10 μm.

mutant brains (Fig. 10c, d). Wts is known to phosphorylate and render Yki inactive, maintaining NSCs in a quiescent state[20,22]. In line with this, the overexpression of a constitutively active form of Yki (Yki^{S168A}) also markedly alleviated NSC reactivation deficits caused by *smt3* or *lwr* depletion: the percentage of EdU-negative quiescent NSCs decreased from 54.3% to 31% (Fig. 10a, b) and 65.7% to 38.1%, in *smt3*- and *lwr*-depleted brains, (Fig. 10c, d), respectively. These data strongly suggest that the SUMO pathway promotes NSC reactivation by inhibiting Wts activity and function (Fig. 10e).

Discussion

Dysregulated SUMOylation is associated with multiple neurodegenerative diseases[75]. For instance, the aggregation of both amyloid-β (Aβ) and the microtubule-associated protein Tau in Alzheimer's disease is closely associated with SUMOylation[76–79]. Similarly, α-synuclein, a key component of Lewy bodies that accumulates in Parkinson's disease, is also known to undergo SUMOylation[78,80]. Our in vivo results in *Drosophila* larval brains showed that loss of function of SUMO or SUMO E2 resulted in decreased number of NSCs and dramatic reduction in brain

https://doi.org/10.1038/s41467-024-52569-y

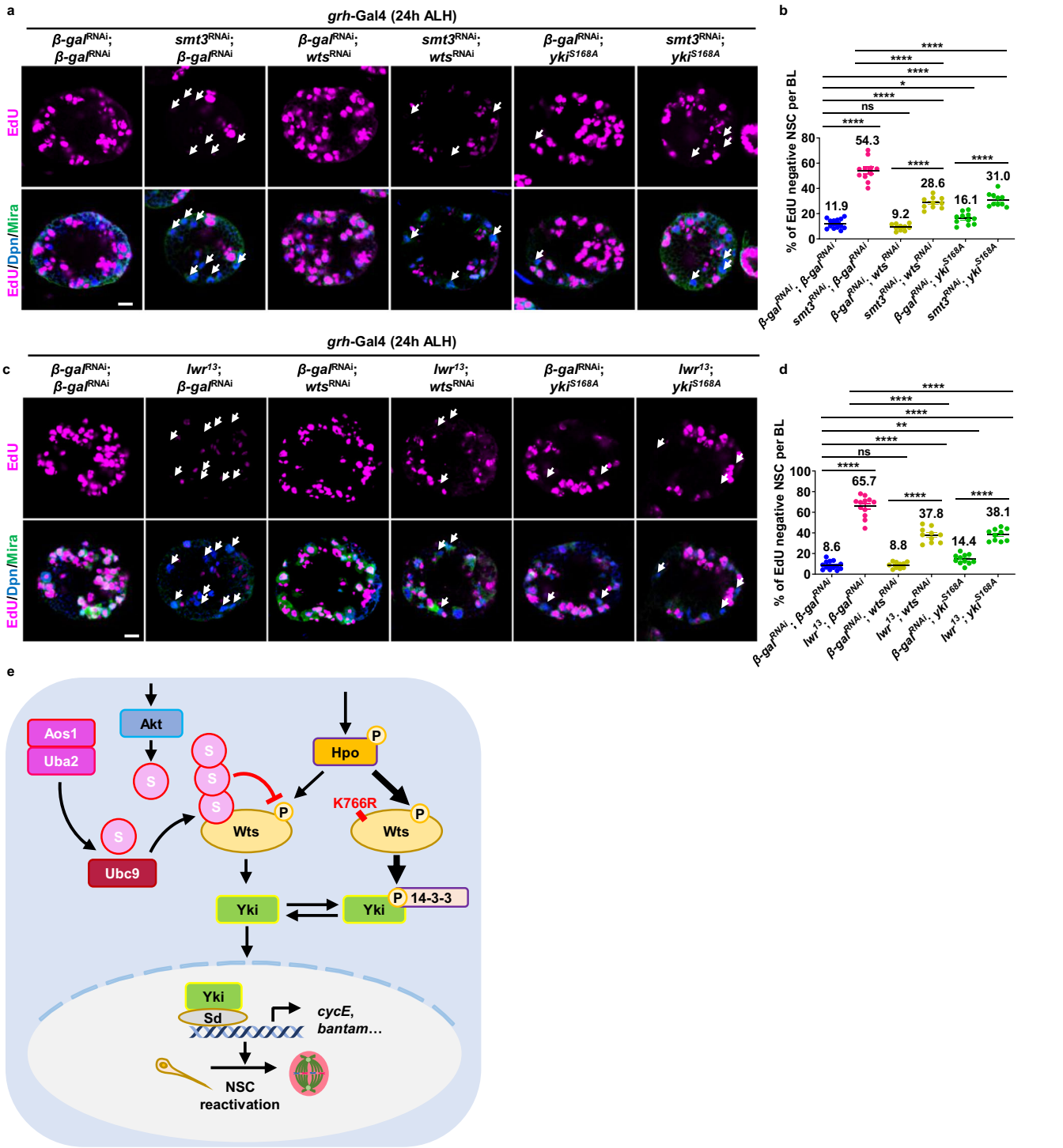

Fig. 10 | SUMO pathway promotes NSC reactivation by inhibiting the Hippo pathway. a, **c** At 24 h ALH, larval brain lobes in indicated genotypes were analyzed for EdU incorporation. NSCs were marked by Dpn and Mira. White arrows point to EdU negative quiescent NSCs. **b**, **d** Quantification graph of EdU- NSCs per BL for genotypes in (**a**, **c**) respectively. **b** Control (*β-gal*^{RNAi}; *β-gal*^{RNAi}), 11.9 ± 3.9, n = 13; *smt3*^{RNAi}; *β-gal*^{RNAi}, 54.3 ± 8.7, P = 1.8E-13, n = 11; *β-gal*^{RNAi}; *wts*^{RNAi}, 9.2 ± 2.5, P = 0.07, n = 10; *smt3*^{RNAi}; *wts*^{RNAi}, 28.6 ± 4.5, P = 4.1E-09, P = 9.3E-08, n = 10; *β-gal*^{RNAi}; *yki*^{S168A}, 16.1 ± 4.6, P = 0.025, n = 10; *smt3*^{RNAi}; *yki*^{S168A}, 31 ± 5.3, P = 1.8E-09, P = 6.5E-07, n = 10. **d** Control (*β-gal*^{RNAi}; *β-gal*^{RNAi}),8.6 ± 4.1, n = 13; *lwr*^{13}; *β-gal*^{RNAi}, 65.7 ± 10, P = 1.6E-15, n = 12; *β-gal*^{RNAi}; *wts*^{RNAi}, 8.8 ± 3, P = 0.89, n = 10; *lwr*^{13}; *wts*^{RNAi}, 37.8 ± 7, P = 3.0E-11, P = 3.9E-07, n = 10; *β-gal*^{RNAi}; *yki*^{S168A}, 14.4 ± 4.7, P = 0.003, n = 11; *lwr*^{13}; *yki*^{S168A}, 38.1 ± 5.7, P = 1.5E-06, P = 2.2E-07, n = 10. Data are presented as mean ± SD. **** for P ≤ 0.0001, ** for P ≤ 0.01 and ns for P > 0.05. Scale bars: 10 μm. **e** A working model illustrating the mechanism by which SUMO pathway promotes NSC reactivation. Wts kinase can be phosphorylated and activated by Hpo kinase. Phosphorylated Wts promotes Yki phosphorylation and cytoplasmic retention. Akt promotes the increase of SUMO protein. SUMO E1 Aos1/Uba2 and E2 Ubc9 promote Wts SUMOylation, resulting in Wts phosphorylation suppression and Wts protein degradation. As a result, Yki phosphorylation is decreased and more non-phosphorylated Yki enters the nucleus and binds to the transcription factor Sd, activating the target genes, such as *cycE* and *bantam* expression and, in turn, promoting quiescent NSC reactivation. P: Phosphate; S: SUMO.

size, mimicking microcephaly phenotypes observed in humans. This potential link between the SUMO pathway and microcephaly warrants further investigation. Interestingly, a newly identified ubiquitin-like protein named ubiquitin-fold modifier 1 (UFM1) and its E2 conjugating enzyme UFC1 were reported in cases of microcephaly in humans[81,82]. Similarly, the murine UFM1 and its specific E3 ligase, and *Drosophila* Ufm1 are known to be essential for brain development and function[83–85].

The *Drosophila* insulin/PI3K/Akt pathway is essential for driving NSC growth and exit from quiescence[18,19]. Here, we show that InR/Akt upregulates SUMO protein level during NSC reactivation. Consistent with our observation, in HEK293T cells, Akt directly phosphorylates SUMO1, leading to its protein stabilization[86]. Interestingly, mammalian Akt is a SUMO substrate, and SUMO modification of Akt is able to promote its activation, suggesting a feedback regulation between Akt and SUMO[86–88].

The *Drosophila* Hippo pathway is central to maintaining the quiescence of NSCs in larval brains[20,22]. The mammalian Hippo pathway plays important roles in central nervous system development, neurodegeneration and neuronal apoptosis[89,90]. Dysregulation of the Hippo pathway can contribute to the initiation and progression of various tumors, including glioma, and neurodegenerative disorders, such as Alzheimer's disease[89–92].

In this study, we have demonstrated a role for SUMOylation in modulating the Wts protein–a key component of the Hippo pathway–during NSC reactivation and brain development. Given that the Hippo pathway only partially suppresses the reactivation deficits, we speculate that the SUMO pathway might regulate additional pathways during quiescent NSC reactivation. One possible candidate could be Akt kinase, as it can be SUMOylated at several Lysine sites in mammalian cells; SUMO modification appears to be crucial for Akt kinase activation and its role in regulating tumorigenesis[86–88].

The SUMOylation of Lats1 at Lys751, which results in the attenuation of its kinase activity, is also conserved in human hepatic cells[93]. Interestingly, the SUMOylation of human Lats1 also leads to destabilization of the phosphorylated Lats1[93]. Intriguingly, we found that the *Drosophila* SUMO pathway negatively regulates Wts protein stability without affecting the stability of phosphorylated Wts. Therefore, Wts SUMOylation and Wts protein stability are controlled in parallel by the SUMOylation pathway. Given that Wts can be ubiquitinated by CRL4 E3 ubiquitin ligase for proteasome degradation[26], the SUMO pathway might indirectly regulate Wts protein stability via modulating the CRL4 E3 ubiquitin ligase function. It is possible that besides SUMOylation, other regulations such as ubiquitination also negatively regulates Wts level in NSCs[26]. This could mitigate the effect of the Wts levels by perturbation of SUMOylation in NSCs.

In summary, our findings have identified SUMO pathway is indispensable for NSC reactivation and brain development in *Drosophila*, underscoring the possibility that a conserved molecular mechanism governing Wts/Lats SUMOylation might impact mammalian NSC proliferation and brain development. Ultimately, our findings may form the basis for the development of promising therapeutic strategies against neurological diseases caused by SUMOylation dysfunction.

Methods

Fly stocks and genetics

Fly stocks and genetic crosses were raised at 25 °C unless otherwise stated. Fly stocks were fed with standard fly food (0.8% *Drosophila* agar, 5.8% Cornmeal, 5.1% Dextrose, and 2.4% Brewer's yeast). The following fly stocks were used in this study: $smt3^{M2L\text{-}2483}$ (Shu Kondo), $smt3^{M2L\text{-}2484}$ (Shu Kondo), $lwr^{M2L\text{-}2401}$(Shu Kondo), $lwr^{M2L\text{-}2402}$(Shu Kondo), *grh*-Gal4 (Andrea Brand), akt^{3} (H. Stocker), *tub*-Gal4, *act*-Gal4, UAS-*venus-smt3* lines (generated in this work), UAS-*venus-*$smt3^{AA}$ lines (generated in this work), UAS-*venus-*wts^{KR} lines (generated in this work). The following fly strains were obtained from BDSC: $smt3^{04493}$(11378), $smt3^{Df24652}$(24652), $\beta\text{-}gal^{RNAi}$ (50680), UAS-CD8-GFP (#32186), $smt3^{RNAi}$-1 (28034), lwr^{RNAi}-1 (31396), $aos1^{c06048}$ (17744), $uba2^{RNAi}$-1 (28569), $uba2^{RNAi}$-2 (35806), lwr^{05486} (11410), lwr^{13} (9323), UAS-*lwr* (9324), UAS-lwr^{DN} (9318), $aos1^{RNAi}$ (36074), UAS-*wts* (44250), $wts^{e26\text{-}1}$(82168), wts^{RNAi} (34064), UAS-yki^{S168A} (28818), Ban-lacZ (10154) and wts^{X1}(44251). RNAi lines including $smt3^{RNAi}$-2 (105980) and lwr^{RNAi}-2 (33685) were obtained from the Vienna *Drosophila* Resource Center (VDRC). Type II driver (w; UAS-*dcr2*; *wor*-Gal4, *ase*-gal80/CyO; UAS-*CD8*:GFP/TM3,Ser) (Juergen). UAS-$\beta\text{-}gal^{RNAi}$ is often used as a control UAS element to balance the total number of UAS elements in each genotype. Various RNAi knockdown or overexpression constructs were induced using *grh*-Gal4 unless otherwise stated. All experiments were carried out at 25 °C, except for RNAi knockdown or overexpression experiments that were performed at 29 °C, unless otherwise indicated.

Screening for NSC lineage development

A collection of CRISPR-Cas9-mediated mutant fly stocks representing 504 genes on chromosome arm 2L[53] was screened by generating MARCM (Mosaic Analysis with a Repressible Cell Marker) clones using the MARCM driver line elav-GAL4; FRT40A, tub-GAL80, UAS-CD8-GFP (Tan Ye Sing and Hongyan Wang, unpublished data). Neural stem cell lineages were labeled by Dpn, Asense, and CD8/GFP. Four mutants, M2L-2483, M2L-2484, M2L-2401 and M2L-2402, displayed a single-cell clone phenotype, suggesting potential defects in NSCs proliferation. These mutants were subjected to further analysis of NSC reactivation via an EdU assay, as detailed in the results.

Generation of plasmids and transgenic flies

Gateway BP, LR Clonase II Enzyme mix (Invitrogen) was used for the generation of entry clone plasmids. cDNA clone of *smt3* (Expressed-sequence tags (EST) LD07775) was obtained from BDGP DGC clones (Berkeley *Drosophila* Genome Project, *Drosophila* Gene Collection). Briefly, genes were amplified by polymerase chain reaction (PCR) first. Then, the amplified fragment was inserted into Gateway vector pDONR221 (Invitrogen) using Gateway BP Clonase II Enzyme mix to generate the entry vector pDONR211-*smt3*. Subsequently, the fragment in the entry vector was inserted into Gateway destination vectors (pTVW, pAMW, pAFW, from Addgene) by LR recombination using Gateway LR Clonase II enzyme mix. Primers used for generating entry clones were as follows:

Smt3 F: GGGG ACA AGT TTG TAC AAA AAA GCA GGC TTC ATGTCTGACGAAAAGAAG

Smt3 R: GGGG AC CAC TTT GTA CAA GAA AGC TGG GTC TTATGGAGCGCCACCAGTCT

Point mutation plasmids were generated using wild-type plasmids as templates, and the PerfectStart® Taq DNA Polymerase kit (TransGen Biotech) was used to perform PCR. The following primers were used for generating point mutation plasmids:

$Smt3^{AA}$ F: TTACCAGCAGCAGACTGCTGCCGCTCCATAA

$Smt3^{AA}$ R: GCAGCAGTCTGCTGCTGGTAAACCTCGATGG

Wts^{K766R} F: GAATCAGGTGGCACACGTGAGGGCCGAGAGGGA

Wts^{K766R} R: CTCACGTGTGCCACCTGATTCCGCTTGAGAAC

Transgenic flies from UAS-*venus-smt3*, UAS-*venus-*$smt3^{AA}$ and UAS-*venus-*wts^{KR} lines were generated by P-element-mediated transformation (BestGene).

Quantitative real-time PCR

Total RNA was isolated from *Drosophila* larva brain with TRI reagent (Sigma Aldrich) followed by DNase I treatment (Sigma-Aldrich) as described by the manufacturer. The quantitative (q)PCR was performed using Maxima SYBR Grebb/ROX qPCR Master Mix (Fermentas) according to the manufacturer's protocol. Primers used here are as below:

Smt3-qF: AGAAGGGAGGTGAGACCGAG
Smt3-qR: GAGTGTCGTTCTCGTTGATG
Wts-qF: GGTCGCCCCAATGATAAATA
Wts-qR: GCGTGGTGATAGTCAGGAGT

EdU (5-ethynyl-20-deoxyuridine) incorporation assay

Larvae were fed with food containing 2% (0.2 mM) EdU from Click-iT EdU Imaging Kits (Invitrogen) for 4 h before dissection. The dissected larval brains were fixed with 4% EM grade formaldehyde for 22 min, followed by washing thrice with 0.3% PBST (PBS + 0.3% Triton-100) and blocking with 3% BSA (bovine serum albumin) in PBST for 45 min. Following blocking, incorporated EdU was detected by Alexa Fluor azide, according to the Click-iT EdU protocol (Invitrogen). The brains were then washed briefly twice, blocked with 3% BSA again for 20 min, and subjected to immunohistochemistry.

Immunohistochemistry

Drosophila larvae were dissected in phosphate-buffered saline (PBS), and the larval brains were fixed in 4% EM-grade formaldehyde in PBST for 22 min. After washing thrice with 0.3% PBT (10 min each), brain samples were blocked with 3% BSA in 0.3% PBST for 45 min. Blocked brain samples were incubated with primary antibodies diluted in 3% BSA overnight at 4 °C. Following this, they were again washed thrice with 0.3% PBST (10 min each) and incubated with secondary antibodies diluted in 0.3% PBT for 1.5 h. DNA was labeled with DAPI (1:1,500, Sigma, 28718-90-3), and after washing twice with 0.3% PBT (10 min each), larval brains were mounted onto Vector shield (Vector Laboratory) for Confocal microscopy. Confocal images were taken by a Zeiss LSM710 confocal microscope and processed with ImageJ for brightness and contrast adjustment. Primary antibodies used were as follows: guinea pig anti-Dpn (1:1,000, J Skeath), mouse anti-Mira (1:50, F. Matsuzaki), rabbit anti-PH3 (1:500, Cell signaling, 9701 L), rabbit anti-SUMO (1:500, Albert J. Courey), rabbit anti-Wts (1:100, generated in this work by Abmart), rabbit anti-GFP (1:3,000, Fengwei Yu), mouse anti-GFP (1:2,000, Fengwei Yu), rabbit anti-Msps (1:1,000, J. Raff), rabbit anti-Yki (1:100, generated by GenScript), mouse anti-β-gal (1:100, Promega, Z378A) and mouse anti-CycE (1:200, H. Richardson). The secondary antibodies used were conjugated with Alexa Fluor 488, 115-545-003, cy3, 111-165-144 or 647, 106-605-003 (Jackson laboratory).

Embryonic staining

The steps for embryo fixation are as follows: the embryos were collected and dechorionated with 50% bleach in PBT for 3 min, followed by a rinse with PBT for 10 min. Embryos were fixed with 4% paraformaldehyde for 15 min. Subsequently, embryos were devitellinized with a mixture of heptane/methanol by shaking vigorously for 60 s followed by washes with methanol and rehydrated with PBT before proceeding with immunostaining, similar to larval brain immunostaining.

Cell lines, transfection and drug treatment

Drosophila S2 cells (CVCL_Z232), originally from William Chia's laboratory, were cultured in Express Five serum-free medium (Gibco) supplemented with 2 mM Glutamine (Thermo Fisher Scientific). For transient expression of proteins, S2 cells were transfected using Effectene Transfection Reagent (QIAGEN) according to the manufacturer's protocol. For RNAi experiments, *Drosophila* S2 cells were cultured and incubated with dsRNA for 72 h. For inhibition of SUMOylation, S2 cells were treated with DMSO as control and the ML-792 (0.2 μM) inhibitor as experiment group for 6 h before harvest. For cycloheximide (CHX) chase assays, S2 cells were treated with CHX at 2 h intervals, with the longest drug treatment being for 6 h.

Protein extraction, immunoprecipitation, immunoblotting and immunofluorescence

S2 cells were transfected with the indicated plasmids and cultured for 48 h; alternately *Drosophila* larval brains were dissected at certain time points, and were collected and lysed in NP-40 lysis buffer along with protease inhibitors (Roche) for 30 min on a rotor at 4 °C. Immunoprecipitation was performed using mouse anti-Flag antibody (1:200, Sigma, F1804-1MG), rabbit anti-Wts (1:50, generated in this work by Abmart), or rat anti-HA (1:100, Roche, 11 867 431 001) and protein G Sepharose beads according to manufacturer's instruction. The samples were separated by SDS–PAGE and analyzed by Western blotting. Blots were probed with the following antibodies: rabbit anti-SUMO (1:500, Albert J. Courey), mouse anti-Flag antibody (1:2000, Sigma, F1804-1MG), mouse anti-Myc antibody (1:2000, abcam, 1011022-8), mouse anti-Tubulin (1:2000, Sigma-Aldrich, T5168), rabbit anti-Wts (1:500, generated in this work by Abmart), rabbit anti-HA (1:2000, Sigma-Aldrich, H6908), rabbit anti-p-Wts (1:500, Duojia Pan), rabbit anti-p-Yki (1:2000, Duojia Pan), and rabbit anti-GAPDH1 (1:500, GeneTex, GTX100118). The secondary antibodies used were conjugated with HRP (Horseradish Peroxidase). For immunofluorescence (IF) assay, cells were transfected with the indicated plasmids after being seeded on coverslips. 48 h later, cells were washed with PBS and fixed in 4% paraformaldehyde for 20 min, and permeabilized with 0.5% Triton X-100 for 30 min at room temperature. Cells were then blocked for 30 min in 3% BSA and incubated with primary antibodies for 2 h, and then with fluorophore-conjugated secondary antibodies for another 1 h at room temperature. They were then treated with DAPI (1:1,500, Sigma, 28718-90-3) for 6 min to mark nuclear DNA before the slides were mounted. Cell images were captured with Zeiss LSM710 Confocal microscope. Antibodies used for IF: rabbit anti-HA (1:1000, Sigma-Aldrich, H6908). The secondary antibody used was conjugated with Alexa Fluor 488 (Jackson laboratory, 115-545-003).

SUMOylation assay

For the SUMOylation assays, the lysis buffer contained NEM protease inhibitor (N-Ethylmaleimide, 10 mM final concentration, Sigma) to inhibit the deconjugating activity of SUMO protease. Protein extracts from S2 cells or larva brains were prepared as described above with SUMO isopeptidase inhibitors NEM, which were then lysed as described above, before carrying out immunoprecipitation and Western blotting.

Generation of anti-Wts antibodies

The N-terminal coding sequence (encoding 1–300 amino acids) of Wts was amplified by PCR and inserted into a GST-containing vector. The purified GST-Wts$^{1-300}$ was then injected into rabbits. Rabbit anti-Wts antibodies were generated and purified by Abmart (Shanghai).

Single cell RNA-seq data analysis

Raw data was downloaded from GSE134722 Brunet et al[62]. and processed by Seurat 4.0. The raw data was firstly analyzed according to the methods in Brunet et al.[62]. Sub-clustering was then performed on the neural stem cells cluster. Quiescent and active neural stem cells were annotated by the expression of proliferating markers: Wor, CycA, CycE and PCNA.

Clonal analysis

MARCM clones were generated as previously described[94]. Briefly, larvae were heat shocked at 37 °C for 90 min twice at 24 h ALH and at 10–16 h after the first heat shock. Larvae were further aged for 3 days at 25 °C, and larval brains were dissected and processed for immunohistochemistry. To generate type II neuroblast clones, UAS lines were crossed to the type II driver at 25 °C and shifted to 18 °C for 44 h, then transfer to 29 °C. Wandering third instar larvae were dissected after incubation for 3 or 4 days at 29 °C.

Quantification and statistical analysis

Statistical analysis was performed using GraphPad Prism 6. *P* values were calculated by performing two-tailed, unpaired Students' T-test. In all graphs, *indicates $0.05 < p < 0.01$, **indicates $p < 0.01$, ***indicates $p < 0.001$, ****indicates $p < 0.0001$, ns indicates $p > 0.05$. Cell population numbers were quantified and represented as mean ± SD and/or percentage of phenotype. Each experiment has at least three independent replications. We distinguish active NSCs from quiescent NSCs based on the cell size, as active NSCs are larger than 7 μm.

Reporting summary

Further information on research design is available in the Nature Portfolio Reporting Summary linked to this article.

Data availability

The authors declare that the data supporting the findings of this study are available within the paper and the source data for figures are provided with the paper. Source data are provided with this paper.

References

1. Morshead, C. M. et al. Neural stem cells in the adult mammalian forebrain: a relatively quiescent subpopulation of subependymal cells. *Neuron* **13**, 1071–1082 (1994).
2. Chiasson, B. J., Tropepe, V., Morshead, C. M. & van der Kooy, D. Adult mammalian forebrain ependymal and subependymal cells demonstrate proliferative potential, but only subependymal cells have neural stem cell characteristics. *J. Neurosci.* **19**, 4462–4471 (1999).
3. Tarpey, P. S. et al. Mutations in CUL4B, which encodes a ubiquitin E3 ligase subunit, cause an X-linked mental retardation syndrome associated with aggressive outbursts, seizures, relative macrocephaly, central obesity, hypogonadism, pes cavus, and tremor. *Am. J. Hum. Genet.* **80**, 345–352 (2007).
4. Zou, Y. et al. Mutation in CUL4B, which encodes a member of cullin-RING ubiquitin ligase complex, causes X-linked mental retardation. *Am. J. Hum. Genet.* **80**, 561–566 (2007).
5. Badura-Stronka, M. et al. A novel nonsense mutation in CUL4B gene in three brothers with X-linked mental retardation syndrome. *Clin. Genet.* **77**, 141–144 (2010).
6. Vulto-van Silfhout, A. T. et al. Variants in CUL4B are associated with cerebral malformations. *Hum. Mutat.* **36**, 106–117 (2015).
7. Vahdatpour, C., Dyer, A. H. & Tropea, D. Insulin-Like Growth Factor 1 and related compounds in the treatment of childhood-onset neurodevelopmental disorders. *Front. Neurosci.* **10**, 450 (2016).
8. Rethelyi, J. M., Vincze, K., Schall, D., Glennon, J. & Berkel, S. The role of insulin/IGF1 signalling in neurodevelopmental and neuropsychiatric disorders - Evidence from human neuronal cell models. *Neurosci. Biobehav. Rev.* **153**, 105330 (2023).
9. Anderson, M. F., Aberg, M. A., Nilsson, M. & Eriksson, P. S. Insulin-like growth factor-I and neurogenesis in the adult mammalian brain.*Dev. Brain Res.* **134**, 115–122 (2002).
10. Plum, L., Schubert, M. & Bruning, J. C. The role of insulin receptor signaling in the brain. *Trends Endocrinol. Metab.* **16**, 59–65 (2005).
11. Wickramasekara, R. N. & Stessman, H. A. F. Histone 4 Lysine 20 Methylation: a case for neurodevelopmental disease. *Biology* **8**, 11 (2019).
12. Ding, W. Y., Huang, J. & Wang, H. Waking up quiescent neural stem cells: molecular mechanisms and implications in neurodevelopmental disorders. *PLoS Genet.* **16**, e1008653 (2020).
13. Otsuki, L. & Brand, A. H. Quiescent neural stem cells for brain repair and regeneration: lessons from model systems. *Trends Neurosci.* **43**, 213–226 (2020).
14. Truman, J. W. & Bate, M. Spatial and temporal patterns of neurogenesis in the central nervous system of *Drosophila* melanogaster. *Dev. Biol.* **125**, 145–157 (1988).
15. Tsuji, T., Hasegawa, E. & Isshiki, T. Neuroblast entry into quiescence is regulated intrinsically by the combined action of spatial Hox proteins and temporal identity factors. *Development* **135**, 3859–3869 (2008).
16. Homem, C. C. & Knoblich, J. A. Drosophila neuroblasts: a model for stem cell biology. *Development* **139**, 4297–4310 (2012).
17. Britton, J. S. & Edgar, B. A. Environmental control of the cell cycle in *Drosophila*: nutrition activates mitotic and endoreplicative cells by distinct mechanisms. *Development* **125**, 2149–2158 (1998).
18. Chell, J. M. & Brand, A. H. Nutrition-responsive glia control exit of neural stem cells from quiescence. *Cell* **143**, 1161–1173 (2010).
19. Sousa-Nunes, R., Yee, L. L. & Gould, A. P. Fat cells reactivate quiescent neuroblasts via TOR and glial insulin relays in *Drosophila*. *Nature* **471**, 508–512 (2011).
20. Ding, R., Weynans, K., Bossing, T., Barros, C. S. & Berger, C. The Hippo signalling pathway maintains quiescence in Drosophila neural stem cells. *Nat. Commun.* **7**, 10510 (2016).
21. Otsuki, L. & Brand, A. H. Cell cycle heterogeneity directs the timing of neural stem cell activation from quiescence. *Science* **360**, 99–102 (2018).
22. Poon, C. L., Mitchell, K. A., Kondo, S., Cheng, L. Y. & Harvey, K. F. The hippo pathway regulates neuroblasts and brain size in drosophila melanogaster. *Curr. Biol.* **26**, 1034–1042 (2016).
23. Huang, J., Wu, S., Barrera, J., Matthews, K. & Pan, D. The Hippo signaling pathway coordinately regulates cell proliferation and apoptosis by inactivating Yorkie, the Drosophila Homolog of YAP. *Cell* **122**, 421–434 (2005).
24. Wu, S., Huang, J., Dong, J. & Pan, D. hippo encodes a Ste-20 family protein kinase that restricts cell proliferation and promotes apoptosis in conjunction with salvador and warts. *Cell* **114**, 445–456 (2003).
25. Goulev, Y. et al. SCALLOPED interacts with YORKIE, the nuclear effector of the hippo tumor-suppressor pathway in Drosophila. *Curr. Biol.* **18**, 435–441 (2008).
26. Ly, P. T. et al. CRL4Mahj E3 ubiquitin ligase promotes neural stem cell reactivation. *PLoS Biol.* **17**, e3000276 (2019).
27. Gil-Ranedo, J. et al. STRIPAK members orchestrate hippo and insulin receptor signaling to promote neural stem cell reactivation. *Cell Rep.* **27**, 2921–2933.e2925 (2019).
28. Huang, J. & Wang, H. Hsp83/Hsp90 physically associates with insulin receptor to promote neural stem cell reactivation. *Stem Cell Rep.* **11**, 883–896 (2018).
29. Li, S. et al. An intrinsic mechanism controls reactivation of neural stem cells by spindle matrix proteins. *Nat. Commun.* **8**, 122 (2017).
30. Huang, J. et al. Histone lysine methyltransferase Pr-set7/SETD8 promotes neural stem cell reactivation. *EMBO Rep.* **22**, e50994 (2021).
31. Gujar, M. R. et al. Patronin/CAMSAP promotes reactivation and regeneration of *Drosophila* quiescent neural stem cells. *EMBO Rep.* **24**, e56624 (2023).
32. Gujar, M. R. et al. Golgi-dependent reactivation and regeneration of *Drosophila* quiescent neural stem cells. *Dev. Cell* **58**, 1933–1949.e5 (2023).
33. Deng, Q., Tan, Y. S., Chew, L. Y. & Wang, H. Msps governs acentrosomal microtubule assembly and reactivation of quiescent neural stem cells. *EMBO J.* **40**, e104549 (2021).
34. Smith, M., Turki-Judeh, W. & Courey, A. J. SUMOylation in *Drosophila* Development. *Biomolecules* **2**, 331–349 (2012).
35. Wilkinson, K. A. & Henley, J. M. Mechanisms, regulation and consequences of protein SUMOylation. *Biochem. J.* **428**, 133–145 (2010).
36. Nayak, A. & Muller, S. SUMO-specific proteases/isopeptidases: SENPs and beyond. *Genome Biol.* **15**, 422 (2014).
37. Smith, M., Bhaskar, V., Fernandez, J. & Courey, A. J. Drosophila Ulp1, a nuclear pore-associated SUMO protease, prevents accumulation

of cytoplasmic SUMO conjugates. *J. Biol. Chem.* **279**, 43805–43814 (2004).
38. Schulman, B. A. & Harper, J. W. Ubiquitin-like protein activation by E1 enzymes: the apex for downstream signalling pathways. *Nat. Rev. Mol. cell Biol.* **10**, 319–331 (2009).
39. Long, X. & Griffith, L. C. Identification and characterization of a SUMO-1 conjugation system that modifies neuronal calcium/calmodulin-dependent protein kinase II in Drosophila melanogaster. *J. Biol. Chem.* **275**, 40765–40776 (2000).
40. Lois, L. M. & Lima, C. D. Structures of the SUMO E1 provide mechanistic insights into SUMO activation and E2 recruitment to E1. *EMBO J.* **24**, 439–451 (2005).
41. Wang, J. et al. Crystal structure of UBA2(ufd)-Ubc9: insights into E1-E2 interactions in Sumo pathways. *PloS ONE* **5**, e15805 (2010).
42. Johnson, E. S. & Blobel, G. Ubc9p is the conjugating enzyme for the ubiquitin-like protein Smt3p. *J. Biol. Chem.* **272**, 26799–26802 (1997).
43. Agrawal, N. & Banerjee, R. Human polycomb 2 protein is a SUMO E3 ligase and alleviates substrate-induced inhibition of cystathionine beta-synthase sumoylation. *PloS ONE* **3**, e4032 (2008).
44. Pichler, A., Gast, A., Seeler, J. S., Dejean, A. & Melchior, F. The nucleoporin RanBP2 has SUMO1 E3 ligase activity. *Cell* **108**, 109–120 (2002).
45. Schmidt, D. & Muller, S. Members of the PIAS family act as SUMO ligases for c-Jun and p53 and repress p53 activity. *Proc. Natl Acad. Sci. USA* **99**, 2872–2877 (2002).
46. Dasso, M. Emerging roles of the SUMO pathway in mitosis. *Cell Div.* **3**, 5 (2008).
47. Zhao, J. Sumoylation regulates diverse biological processes. *Cell. Mol. Life Sci.* **64**, 3017–3033 (2007).
48. Yau, T. Y., Molina, O. & Courey, A. J. SUMOylation in development and neurodegeneration. *Development* **147**, dev175703 (2020).
49. Eckermann, K. SUMO and Parkinson's disease. *Neuromol. Med.* **15**, 737–759 (2013).
50. Knock, E. et al. SUMO1 impact on Alzheimer disease pathology in an amyloid-depositing mouse model. *Neurobiol. Dis.* **110**, 154–165 (2018).
51. Anderson, D. B., Zanella, C. A., Henley, J. M. & Cimarosti, H. Sumoylation: implications for neurodegenerative diseases. *Adv. Exp. Med. Biol.* **963**, 261–281 (2017).
52. Wilkinson, K. A., Nakamura, Y. & Henley, J. M. Targets and consequences of protein SUMOylation in neurons. *Brain Res. Rev.* **64**, 195–212 (2010).
53. Nagata, R. et al. Yorkie drives supercompetition by non-autonomous induction of autophagy via bantam microRNA in Drosophila. *Curr. Biol.* **32**, 1064–1076.e1064 (2022).
54. Nie, M., Xie, Y., Loo, J. A. & Courey, A. J. Genetic and proteomic evidence for roles of Drosophila SUMO in cell cycle control, Ras signaling, and early pattern formation. *PLoS ONE* **4**, e5905 (2009).
55. Johnson, E. S. Protein modification by SUMO. *Annu. Rev. Biochem.* **73**, 355–382 (2004).
56. Apionishev, S., Malhotra, D., Raghavachari, S., Tanda, S. & Rasooly, R. S. The Drosophila UBC9 homologue lesswright mediates the disjunction of homologues in meiosis I. *Genes Cells* **6**, 215–224 (2001).
57. Monribot-Villanueva, J. et al. TnaA, an SP-RING protein, interacts with Osa, a subunit of the chromatin remodeling complex BRAHMA and with the SUMOylation pathway in Drosophila melanogaster. *PLoS ONE* **8**, e62251 (2013).
58. Tashiro, K. et al. Direct involvement of the ubiquitin-conjugating enzyme Ubc9/Hus5 in the degradation of IkappaBalpha. *Proc. Natl Acad. Sci. USA* **94**, 7862–7867 (1997).
59. Huang, L., Ohsako, S. & Tanda, S. The lesswright mutation activates Rel-related proteins, leading to overproduction of larval hemocytes in Drosophila melanogaster. *Dev. Biol.* **280**, 407–420 (2005).
60. Thibault, S. T. et al. A complementary transposon tool kit for Drosophila melanogaster using P and piggyBac. *Nat. Genet.* **36**, 283–287 (2004).
61. Kanakousaki, K. & Gibson, M. C. A differential requirement for SUMOylation in proliferating and non-proliferating cells during Drosophila development. *Development* **139**, 2751–2762 (2012).
62. Brunet Avalos, C., Maier, G. L., Bruggmann, R. & Sprecher, S. G. Single cell transcriptome atlas of the Drosophila larval brain. *Elife* **8**, e50354 (2019).
63. Li, S. et al. The SCFSlimb E3 ligase complex regulates asymmetric division to inhibit neuroblast overgrowth. *EMBO Rep.* **15**, 165–174 (2014).
64. Beauclair, G., Bridier-Nahmias, A., Zagury, J. F., Saib, A. & Zamborlini, A. JASSA: a comprehensive tool for prediction of SUMOylation sites and SIMs. *Bioinformatics* **31**, 3483–3491 (2015).
65. Yang, S. H., Galanis, A., Witty, J. & Sharrocks, A. D. An extended consensus motif enhances the specificity of substrate modification by SUMO. *EMBO J.* **25**, 5083–5093 (2006).
66. Matic, I. et al. Site-specific identification of SUMO-2 targets in cells reveals an inverted SUMOylation motif and a hydrophobic cluster SUMOylation motif. *Mol. Cell* **39**, 641–652 (2010).
67. Desterro, J. M., Rodriguez, M. S., Kemp, G. D. & Hay, R. T. Identification of the enzyme required for activation of the small ubiquitin-like protein SUMO-1. *J. Biol. Chem.* **274**, 10618–10624 (1999).
68. Chen, W. Y., Lee, W. C., Hsu, N. C., Huang, F. & Chung, B. C. SUMO modification of repression domains modulates function of nuclear receptor 5A1 (steroidogenic factor-1). *J. Biol. Chem.* **279**, 38730–38735 (2004).
69. He, X. et al. Probing the roles of SUMOylation in cancer cell biology by using a selective SAE inhibitor. *Nat. Chem. Biol.* **13**, 1164–1171 (2017).
70. Chan, E. H. et al. The Ste20-like kinase Mst2 activates the human large tumor suppressor kinase Lats1. *Oncogene* **24**, 2076–2086 (2005).
71. Zhang, L. et al. The TEAD/TEF family of transcription factor Scalloped mediates Hippo signaling in organ size control. *Dev. Cell* **14**, 377–387 (2008).
72. Pojer, J. M., Manning, S. A., Kroeger, B., Kondo, S. & Harvey, K. F. The Hippo pathway uses different machinery to control cell fate and organ size. *iScience* **24**, 102830 (2021).
73. Le, N. T., Martin, J. F., Fujiwara, K. & Abe, J. I. Sub-cellular localization specific SUMOylation in the heart. *Biochim Biophys. Acta Mol. Basis Dis.* **1863**, 2041–2055 (2017).
74. Li, W. et al. Merlin/NF2 loss-driven tumorigenesis linked to CRL4(DCAF1)-mediated inhibition of the hippo pathway kinases Lats1 and 2 in the nucleus. *Cancer Cell* **26**, 48–60 (2014).
75. Zheng, C., Geetha, T. & Babu, J. R. Failure of ubiquitin proteasome system: risk for neurodegenerative diseases. *Neurodegener. Dis.* **14**, 161–175 (2014).
76. Zhang, Y. Q. & Sarge, K. D. Sumoylation of amyloid precursor protein negatively regulates Abeta aggregate levels. *Biochem. Biophys. Res. Commun.* **374**, 673–678 (2008).
77. Li, Y. et al. Positive and negative regulation of APP amyloidogenesis by sumoylation. *Proc. Natl Acad. Sci. USA* **100**, 259–264 (2003).
78. Dorval, V. & Fraser, P. E. Small ubiquitin-like modifier (SUMO) modification of natively unfolded proteins tau and alpha-synuclein. *J. Biol. Chem.* **281**, 9919–9924 (2006).
79. Luo, H. B. et al. SUMOylation at K340 inhibits tau degradation through deregulating its phosphorylation and ubiquitination. *Proc. Natl Acad. Sci. USA* **111**, 16586–16591 (2014).

80. Abeywardana, T. & Pratt, M. R. Extent of inhibition of alpha-synuclein aggregation in vitro by SUMOylation is conjugation site- and SUMO isoform-selective. *Biochemistry* **54**, 959–961 (2015).
81. Nahorski, M. S. et al. Biallelic UFM1 and UFC1 mutations expand the essential role of ufmylation in brain development. *Brain* **141**, 1934–1945 (2018).
82. Hamilton, E. M. C. et al. UFM1 founder mutation in the Roma population causes recessive variant of H-ABC. *Neurology* **89**, 1821–1828 (2017).
83. Muona, M. et al. Biallelic variants in UBA5 link dysfunctional UFM1 Ubiquitin-like modifier pathway to severe infantile-onset encephalopathy. *Am. J. Hum. Genet.* **99**, 683–694 (2016).
84. Yu, L. et al. The UFM1 cascade times mitosis entry associated with microcephaly. *FASEB J.* **34**, 1319–1330 (2020).
85. Zhang, J. et al. Deficiency of Murine UFM1-Specific E3 ligase causes microcephaly and inflammation. *Mol. Neurobiol.* **59**, 6363–6372 (2022).
86. Lin, C. H., Liu, S. Y. & Lee, E. H. SUMO modification of Akt regulates global SUMOylation and substrate SUMOylation specificity through Akt phosphorylation of Ubc9 and SUMO1. *Oncogene* **35**, 595–607 (2016).
87. Li, R. et al. Akt SUMOylation regulates cell proliferation and tumorigenesis. *Cancer Res.* **73**, 5742–5753 (2013).
88. Risso, G. et al. Modification of Akt by SUMO conjugation regulates alternative splicing and cell cycle. *Cell Cycle* **12**, 3165–3174 (2013).
89. Ouyang, T., Meng, W., Li, M., Hong, T. & Zhang, N. Recent advances of the Hippo/YAP signaling pathway in brain development and Glioma. *Cell Mol. Neurobiol.* **40**, 495–510 (2020).
90. Sahu, M. R. & Mondal, A. C. The emerging role of Hippo signaling in neurodegeneration. *J. Neurosci. Res.* **98**, 796–814 (2020).
91. Elmore, S. Apoptosis: a review of programmed cell death. *Toxicol. Pathol.* **35**, 495–516 (2007).
92. Ostrom, Q. T., Gittleman, H., Stetson, L., Virk, S. M. & Barnholtz-Sloan, J. S. Epidemiology of gliomas. *Cancer Treat. Res.* **163**, 1–14 (2015).
93. Mei, L. et al. SUMOylation of large tumor suppressor 1 at Lys751 attenuates its kinase activity and tumor-suppressor functions. *Cancer Lett.* **386**, 1–11 (2017).
94. Lee, T. & Luo, L. Mosaic analysis with a repressible cell marker for studies of gene function in neuronal morphogenesis. *Neuron* **22**, 451–461 (1999).

Acknowledgements

We thank Duojia Pan, Jin Jiang, Fengwei Yu, Shian Wu, Albert J. Courey, Katalin Fejes, H. Richardson and the Bloomington *Drosophila* Stock Center, Vienna *Drosophila* Resource Center, Kyoto Stock Centre DGGR, and the Developmental Studies Hybridoma Bank, Abmart INC for plasmids, fly stocks and antibodies, and Ravinuthula Sruthi Jagannathan for comments on this manuscript. This work is supported by the Ministry of Health-Singapore National Medical Research Council funding schemes MOH-000143 to Hongyan Wang and MOH-000924 to Y.G.

Author contributions

Conceptualization, Y.G. and H.W.; methodology, data curation, and formal analysis, Y.G., Y.S.T., J.L., L.Y.C., H.Y.A., B.P., M.R.G. and K.Y.L.; writing – original draft, writing – review and editing, Y.G., M.R.G. and H.W.; funding acquisition, H.W. and Y.G.; resources, H.W. and S.K.; supervision, H.W.

Competing interests

The authors declare no competing interests.

Additional information

Supplementary information The online version contains supplementary material available at https://doi.org/10.1038/s41467-024-52569-y.

Correspondence and requests for materials should be addressed to Hongyan Wang.

Peer review information *Nature Communications* thanks the anonymous reviewers for their contribution to the peer review of this work. A peer review file is available.